MOLECULAR BIOLOGY

HMCES corrupts replication fork stability during base excision repair in homologous recombination–deficient cells

María José Peña-Gómez[1,2], Yaiza Rodríguez-Martín[1,2], Marta del Rio Oliva[1,2], Yodhara Wijesekara Hanthi[3,4], Sara Berrada[5,6], Raimundo Freire[7,8,9], Jean Yves Masson[5,6], José Carlos Reyes[1], Vincenzo Costanzo[3,4], Iván V. Rosado[1,2]*

Apurinic/apyrimidinic (AP) sites and single-strand breaks arising from base excision repair (BER) during the misincorporation of damaged nucleobases may hinder replication fork stability in homologous recombination–deficient (HRD) cells. At templated AP sites, cross-links between the DNA and 5-hydroxymethylcytosine binding, embryonic stem cell–specific (HMCES) regulate replication fork speed, avoiding cytotoxic double-strand breaks. While the role of HMCES at the template DNA strand is well studied, its effects on nascent DNA are not. We provide evidence that HMCES–DNA-protein cross-links (DPCs) are detrimental to the BER-mediated removal of 5-hydroxymethyl-2′-deoxycytidine (5hmdC)–derived 5-hydroxymethyl-2′-deoxyuridine from replication forks. HRD cells have heightened HMCES-DPCs, which increase further upon 5hmdC exposure, suggesting that HMCES binds both spontaneous and 5hmdC-induced AP sites. HMCES depletion substantially suppresses 5hmdC-mediated replication fork defects, chromosomal aberrations, and cell death in HRD cells. This reveals that HMCES-DPCs are a source of BER-initiated single-stranded DNA gaps, which indicates that endogenous DPCs contribute to genomic instability in HRD tumors.

INTRODUCTION

Chemical or physical modifications of DNA bases, in addition to uracil (and its derivative forms) misincorporation, are perhaps the major source of DNA lesions in cells. These harmful DNA lesions appear at an estimated frequency of 1×10^5 to 5×10^5 cell^{-1} day^{-1} (*1*). During the repair of those lesions, apurinic/apyrimidinic (AP) sites are formed by DNA glycosylase activity. To avoid their deleterious consequences due to their intrinsic chemical instability, AP sites are rapidly converted to single-strand breaks (SSBs) by either the AP lyase or the AP endonuclease (APEX) activities of certain class of nucleases. Therefore, the repair of base alterations, AP sites, and SSBs is perhaps the most important process responding to oxidative and alkylating base damages (*2*, *3*). More intriguingly is how these damaged bases are repaired by base excision repair (BER) in the context of replication forks. This is of utmost relevance as AP sites and SSBs are potent replication fork–blocking lesions, which, if left unrepaired, hinder replication fork stability. Moreover, the persistence of single-stranded DNA (ssDNA) gaps behind replication forks is relevant in the clinic to eradicate homologous recombination–deficient (HRD) tumors, as they are efficiently targeted by poly(adenosine 5′-diphosphate–ribose) polymerase (PARP) inhibitors. For these reasons, understanding ssDNA gap formation caused by BER activity is of paramount interest in the context of HRD, as many factors involved in HR [breast cancer gene 1 (BRCA1), breast cancer gene 2 (BRCA2), radiation sensitive protein 51 (RAD51), fanconi anemia group D2 (FANCD2), etc.] are also crucial for replication fork maintenance.

Misincorporation of damaged nucleotides and depurination of adducted bases are among the most common spontaneous base lesions in DNA (*1*, *4*–*6*), triggering canonical BER (*7*, *8*). During damaged base removal, AP sites generated by DNA glycosylases [e.g., single-strand selective mo nofunctional uracil DNA glycosylase (SMUG1) during 5-hydroxymethyl-2′-deoxyuridine (5hmdU) excision] are converted to SSBs by APEX1. Upon DNA end processing, DNA polymerase β or λ conducts gap filling, leaving nicked DNA ready for ligation by the x-ray repair cross-complementing 1 (XRCC1)/DNA ligase 1 or ligase 3 complexes (*9*–*11*). Despite the "passing-the-baton" model of BER, where DNA intermediates are passed along from one step to the next, AP sites or SSBs may persist and challenge replication fork progression, eliciting a replication stress (RS) response. Upon replication fork stalling by DNA intermediates, ataxia telangiectasia and Rad3-related (ATR) accelerates recruitment and stabilization of critical components of the DNA damage response, such as the Fanconi anemia (FA) pathway and the HR factors FANCD2/FANCI-associated nuclease 1 (FAN1), structure-specific endonuclease (SLX4), xeroderma pigmentosum F (XPF), BRCA1/2, or RAD51. To fulfill DNA synthesis, the primase-polymerase (PRIMPOL) reprimes ahead of both the stalled replication fork and the lesion to limit replication fork instability, thus dampening RS (*12*–*14*). However, PRIMPOL activity generates potentially cytotoxic ssDNA gaps behind forks (*15*–*18*), which are subsequently filled in either by REV1-POLζ translesion synthesis (TLS) polymerases or by POLQ (*19*–*21*). Several mechanisms have been recently proposed as major contributors to HRD cell lethality. The unifying feature among them is the

[1]Centro Andaluz de Biología Molecular y Medicina Regenerativa (CABIMER) Universidad de Sevilla-CSIC-Universidad Pablo de Olavide, Seville 41092, Spain. [2]Departamento de Genética, Facultad de Biologia, Universidad de Sevilla, Seville 41012, Spain. [3]IFOM, The AIRC Institute of Molecular Oncology, Milan, Italy. [4]Department of Oncology and Hematology-Oncology, University of Milan, Milan, Italy. [5]Genome Stability Laboratory, CHU de Québec Research Center, HDQ Pavilion, Oncology Division, 9 McMahon, Québec City, QC G1R 3S3, Canada. [6]Department of Molecular Biology, Medical Biochemistry and Pathology, Laval University Cancer Research Center, Québec City, QC G1V 0A6, Canada. [7]Unidad de Investigación, Hospital Universitario de Canarias, Instituto de Investigación Sanitaria de Canarias (IISC), La Laguna, Santa Cruz de Tenerife, Spain. [8]Instituto de Tecnologías Biomédicas, Centro de Investigaciones Biomédicas de Canarias, Facultad de Medicina, Campus Ciencias de la Salud, Universidad de La Laguna, Santa Cruz de Tenerife, Spain. [9]Universidad Fernando Pessoa Canarias, Las Palmas de Gran Canaria, Spain.
*Corresponding author. Email: ivrosado@us.es

presence of persistent ssDNA gaps at nascent DNA strands, which correlates with the exquisite cytotoxicity to PARP inhibitors (e.g., olaparib) observed in HRD cells (*22*, *23*). However, the underlying molecular basis of this cytotoxicity still remains elusive.

Recently, misincorporation of dU, 5′-chloro-dU (5CldU), or 5hmdU has emerged as a previously unidentified source of replication fork impairment (*24*–*27*). Upon misincorporation, persisting DNA repair intermediate structures can be collided by the replisome, resulting in BER-replication conflicts (BRCs). These unresolved BRCs account for HRD cell death in the absence of proficient replication fork maintenance or HR pathways (*24*–*27*). In addition, modified DNA bases remaining undetectable throughout the cell cycle induce an ATR-dependent RS and fork collapse response during the next cell cycle when present in template DNA (*28*, *29*). Whereas ssDNA gap accumulation by BRCs during the next cell cycle is well documented (*12*, *30*–*33*), how ssDNA gaps arise at nascent DNA during the current cell cycle remains largely unexplored (*25*, *26*).

Damaged DNA bases are one of the main sources of AP sites. On template DNA, AP sites are exposed during DNA unwinding by Cdc45–MCM–GINS (CMG) helicase and are protected by the 5-hydroxymethylcytosine binding, embryonic stem cell–specific (HMCES) protein (*34*–*39*). Through its interaction with proliferating cell nuclear antigen (PCNA), HMCES associates to replication forks and binds ssDNA to shield AP sites (*34*, *35*). Through a thiazolidine bond between the Cys2 residue and the aldehydic conformation of the AP site (*34*–*36*, *40*), HMCES attaches covalently to AP sites, forming an HMCES–DNA-protein cross-links (DPC). HMCES-DPC formation on template ssDNA decreases replication fork speed while avoiding APEX1-mediated cytotoxic double-strand breaks (DSBs) at replication forks (*35*). HMCES-DPCs are bypassed by a TLS step and subsequently removed from DNA by distinct mechanisms. Upon winding of DNA strands, HMCES-DPC catalyzes a cross-link self-reversal reaction through its Glu127 residue, releasing HMCES from DNA (*37*, *38*). Alternatively, assisted by the protein denaturation activity of fanconi anemia group J (FANCJ) (*39*), SprT-like N-terminal domain (SPTRN) or proteasome degrades HMCES to allow replication fork resumption (*35*, *39*). While the consequences of HMCES-DPCs on template DNA are recently being addressed, the effects on nascent DNA are unknown. Here, we provide evidence of a detrimental role of HMCES-DPCs during nascent DNA synthesis. HRD cells display heightened chromatin levels of HMCES, which increase upon 5-hydroxymethyl-2′-deoxycytidine (5hmdC) exposure, suggesting that HMCES binds to spontaneous and 5hmdU-induced AP sites. HMCES loss rescues replication fork impairment, genomic instability, and cytotoxic phenotypes observed in HRD cells during 5hmdU misincorporation, indicating that HMCES is responsible for the 5hmdU-mediated genetic instability and lethality of HRD cells. Genetic depletion of ssDNA gap–generating BER factors (e.g., SMUG1 or APEX1/2) largely suppresses these phenotypes, whereas loss of ssDNA gap–filling factors PARP1 or XRCC1 exacerbates them. Our findings demonstrate that HMCES-DPCs on nascent DNA are responsible for the replication fork defects observed in HRD-deficient cells and place endogenous DPCs on nascent DNA as a novel source of genomic instability in HRD tumors.

RESULTS

Misincorporation of 5hmdU arising from deaminated 5hmdC causes genomic instability in HRD cells

5hmdU can arise from either the 5hmdC salvage pathway or the cytosine demethylation process (*24*, *25*, *27*). Previous data from our group and others have shown that HRD cells lacking FANCD2, methyl methanesulfonate and UV sensitive protein 81 (MUS81), BRCA1, or BRCA2 were sensitive to misincorporation of 5hmdU on genomic DNA (*25*, *27*). To investigate the molecular mechanisms accounting for 5hmdU-mediated genotoxicity, we examined whether depletion of factors involved in the pyrimidine salvage pathway [e.g., deoxycytidine kinase (DCK) or 2′-deoxycytidine 5′-monophosphate deaminase (DCTD)] had any effect on the viability of 5hmdC-treated *Fancd2*$^{-/-}$ mouse embryonic fibroblasts (MEFs). Consistent with previous results in human HRD cells (*25*, *27*), 5hmdC-mediated *Fancd2*$^{-/-}$ lethality was largely suppressed by knockdown of DCK or DCTD, whereas wild-type cells remained unaltered (Fig. 1A and fig. S1), confirming that deamination of 5hmdC to 5hmdU mediates HRD cell cytotoxicity. As PARP trapping by olaparib exacerbated 5hmdC-dependent *Fancd2*$^{-/-}$ chromosomal instability and cell lethality (*25*), we sought to determine levels of nuclear PARylation and SSBs upon 5hmdC treatment. As expected, *Fancd2*$^{-/-}$ ethynyl-2′-deoxyuridine–positive (EdU^{+}) cells displayed a significant increase in nuclear PARylation (Fig. 1B), also confirmed in EdU unrestricted cells (fig. S2A), while it remained relatively unchanged in wild-type cells (Fig. 1B and fig. S2A). Next, we examined PAR levels associated with ongoing replication forks by "in situ protein interaction with nascent DNA replication forks" also known as SIRF assay. Compared to wild-type MEFs, *Fancd2*$^{-/-}$ cells displayed heightened EdU-PAR foci, which were further exacerbated by 5hmdC treatment (Fig. 1C). The increase in nuclear PARylation or EdU-PAR foci observed in *Fancd2*$^{-/-}$ cells was largely dependent on PARP1, as PARP1 knockdown significantly reduced both PARylation and EdU-PAR foci (Fig. 1, B and C). *Fancd2*$^{-/-}$ MEFs also displayed significant spontaneous SSBs measured by alkaline comet assay, which were further increased by 5hmdC treatment, unlike in wild-type cells (Fig. 1D). These data suggest that 5hmdU misincorporation results in ssDNA gap accumulation in the absence of FANCD2, probably accounting for heightened PARylation at replication forks. Consistent with this, we also found that 5hmdC exposure caused increased replication fork asymmetry by DNA fiber assay (Fig. 1E), indicating that 5hmdU-dependent replication fork impairment was not a consequence of a global checkpoint response. Moreover, 5hmdU-mediated DNA damage increased sister chromatid exchanges (SCEs) in *Fancd2*$^{-/-}$ cells (Fig. 1F), suggesting that BRCs elicited an HR-dependent repair mechanism. However, we did not observe any evidence of checkpoint activation measured as Ser345-CHEK1 or Ser33-RPA2 under these conditions (fig. S3). These data suggest that short 5hmdC exposure does not activate the DNA damage checkpoint despite increased SSBs and indicate that ssDNA gaps arising during 5hmdU removal trigger replication fork impairment and sister chromatid recombination in HRD cells.

ssDNA gaps arising from the concerted activities of SMUG1 and APEX1/2 on misincorporated 5hmdU alter replication fork progression

Previous studies have reported ssDNA gap accumulation as a major contributor to BRCA1/2 tumor cell death (*18*, *31*, *41*). As SMUG1 is the main BER DNA glycosylase responsible for 5hmdU elimination from genomic DNA (*42*), we sought to examine its contribution to ssDNA gap formation in nascent DNA. In agreement with a previous report (*27*), SMUG1 depletion in 5hmdC-treated *Fancd2*$^{-/-}$ cells significantly decreased nuclear PARylation to untreated levels in both total and EdU^{+} cells compared to wild-type cells (Fig. 2A and fig. S2B). SMUG1 depletion suppressed 5hmdC-dependent EdU-PAR

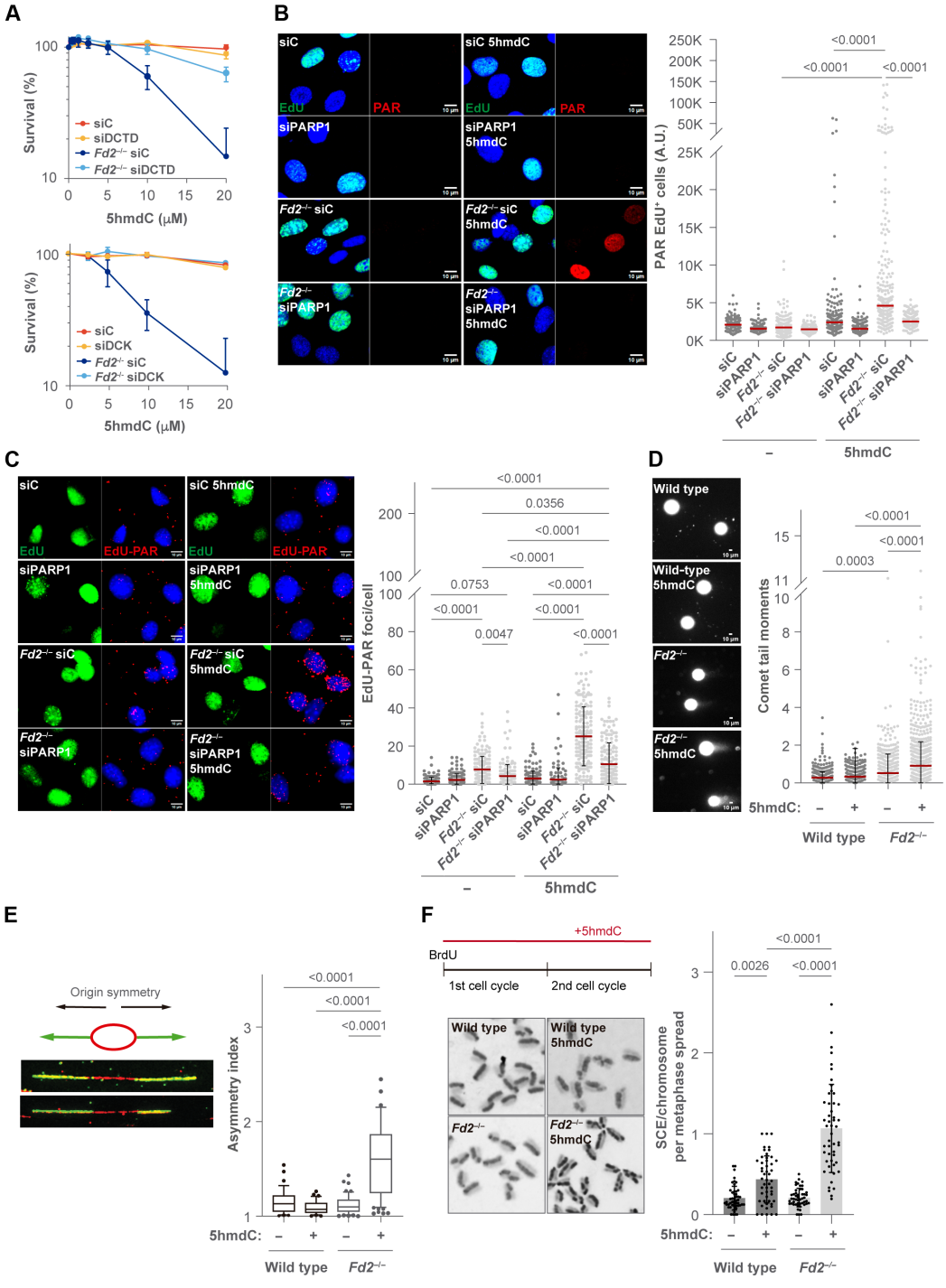

Fig. 1. Genomic instability induced by 5hmdC in HRD cells. (**A**) (3-(4, 5-dimethylthiazolyl-2)-2, 5-diphenyltetrazolium bromide) assay (MTT) cell proliferation assay of 5hmdC-treated wild-type or *Fancd2*$^{-/-}$ (*Fd2*$^{-/-}$) cells knocked down for DCTD (top) or DCK (bottom) exposed to the indicated dose for 3 days. (**B**) Left: Representative PAR (red) immunofluorescence images of EdU^{+} (green) wild-type, siPARP1, *Fancd2*$^{-/-}$, and *Fancd2*$^{-/-}$ siPARP1 cells exposed to 5hmdC (10 μM) for 3 hours. 4′,6-Diamidino-2-phenylindole (DAPI; blue) stains nuclear DNA. Right: Plot depicting PAR mean intensity signal per nucleus. A.U., arbitrary units. (**C**) Left: Representative images of EdU^{+}-PAR foci (red) by SIRF analysis from wild-type, siPARP1, *Fancd2*$^{-/-}$, and *Fancd2*$^{-/-}$ siPARP1 cells exposed to 5hmdC (10 μM) for 3 hours. DAPI (blue) stains nuclear DNA and EdU (green) stains S-phase cells. Right: Plot depicting EdU-PAR foci per nucleus ($n = 2$). (**D**) Left: Representative images of alkaline comet assay from wild-type and *Fancd2*$^{-/-}$ cells following 5hmdC treatment (10 μM) for 3 hours. Right: Plot depicting comet tail moment per cell ($n = 4$). (**E**) Top left: Scheme of the DNA fiber origin symmetry. Bottom left: Representative images of DNA fibers from wild-type and *Fancd2*$^{-/-}$ cells upon 5hmdC treatment (40 μM) for 30 min. Right: Box plot of the asymmetry index. (**F**) Top left: Scheme of SCE assay. Bottom left: Representative images of SCEs from wild-type and *Fancd2*$^{-/-}$ cells exposed to 5hmdC (10 μM) for 40 hours. Right: Bar plot of SCE/chromosome per metaphase spread ($n = 50$ of each of the two biological replicates; bar represents means ± SD). BrdU, 5-bromo-2′-deoxyuridine.

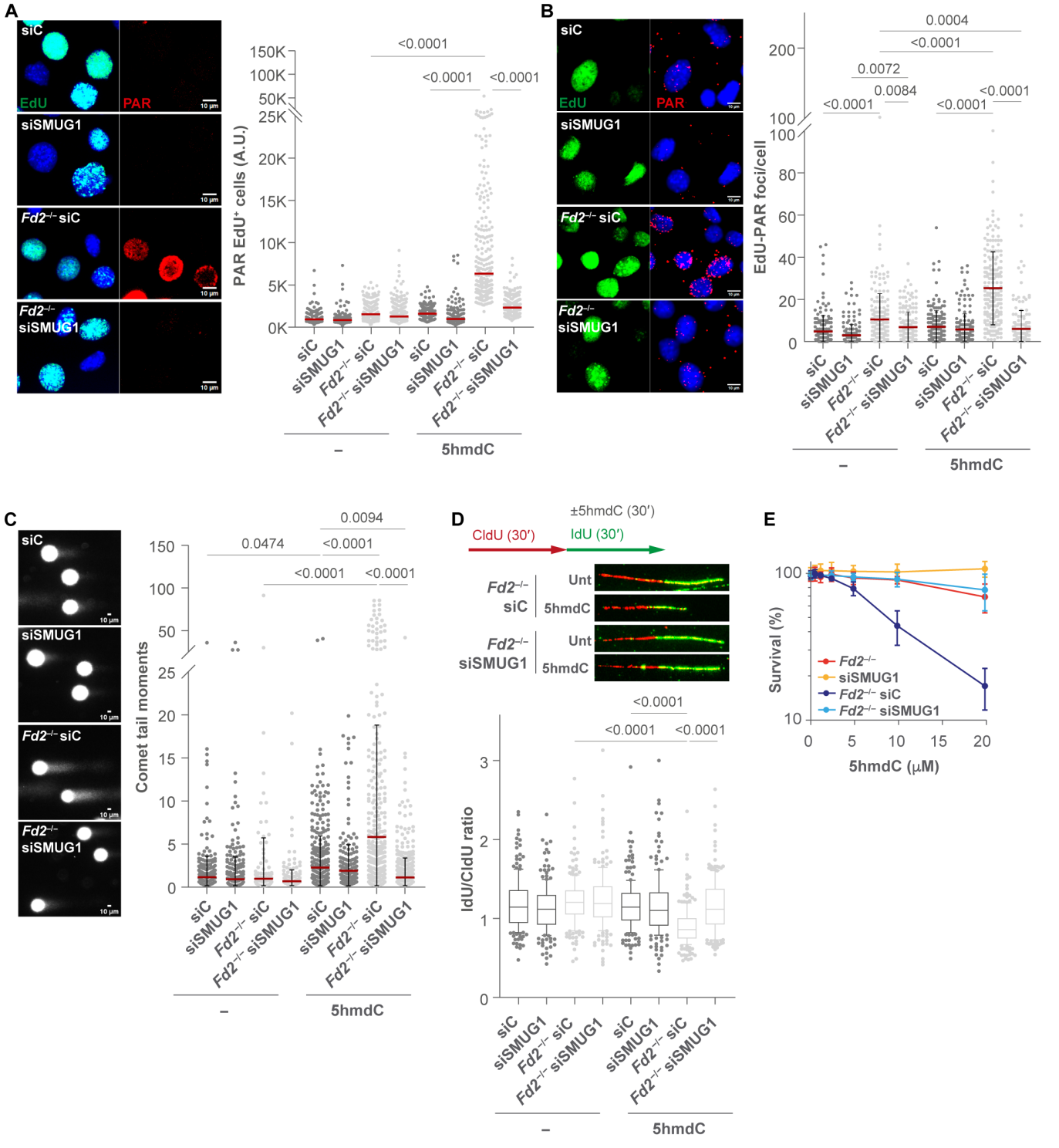

Fig. 2. 5hmdC-mediated HRD genomic instability is dependent on SMUG1. (**A**) Left: Representative PAR (red) immunofluorescence images of EdU^{+} (green) wild-type, siSMUG1, *Fancd2*$^{-/-}$, and *Fancd2*$^{-/-}$ siSMUG1 cells exposed to 5hmdC (10 μM) for 3 hours. DAPI (blue) stains nuclear DNA. Right: Plot depicting PAR mean intensity signal per nucleus. (**B**) Left: Representative images of EdU-PAR foci (red) by SIRF assay from wild-type, siSMUG1, *Fancd2*$^{-/-}$, and *Fancd2*$^{-/-}$ siSMUG1 cells exposed to 5hmdC (10 μM) for 3 hours. DAPI (blue) stains nuclear DNA and EdU (green) stains S-phase cells. Right: Plot depicting EdU-PAR foci per nucleus ($n = 2$). (**C**) Left: Representative images of alkaline comet assay from wild-type, siSMUG1, *Fancd2*$^{-/-}$, and *Fancd2*$^{-/-}$ siSMUG1 cells following 5hmdC treatment (10 μM) for 3 hours. Right: Plot depicting comet tail moment per cell ($n = 2$). (**D**) Top left: Scheme of DNA fiber assay. Bottom left: Representative images of DNA fibers from *Fancd2*$^{-/-}$ and *Fancd2*$^{-/-}$ siSMUG1 cells untreated (Unt) or exposed to 5hmdC (40 μM) for 30 min. Right: Box plot representing the frequency of 5′-iododeoxyuridine (IdU)/CldU ratio of wild-type, siSMUG1, *Fancd2*$^{-/-}$, and *Fancd2*$^{-/-}$ siSMUG1 cells after 5hmdC treatment ($n = 200$). (**E**) MTT cell proliferation assay of wild-type, siSMUG1, *Fancd2*$^{-/-}$, and *Fancd2*$^{-/-}$ siSMUG1 cells exposed to the indicated dose of 5hmdC for 3 days ($n = 4$; means ± SD).

foci to untreated levels (Fig. 2B), suggesting that most replication fork–associated PARylation upon 5hmdC exposure depends on SMUG1. Consistent with this, SMUG1 knockdown also abolished 5hmdC-induced SSBs in *Fancd2*$^{-/-}$ cells (Fig. 2C), suggesting that SMUG1 is responsible for 5hmdC-induced ssDNA gap formation. Moreover, SMUG1 depletion largely restored replication fork progression measured by DNA fiber assay and cell viability in 5hmdC-treated *Fancd2*$^{-/-}$ cells (Fig. 2, D and E). These data demonstrate that SMUG1 loss suppresses ssDNA gap accumulation, replication fork impairment, and lethality observed in 5hmdC-treated HRD cells, most likely throughout the abolishment of AP site formation.

Mammalian cells contain two class II APEXs, APEX1 and APEX2 (*43*, *44*). While APEX1 has strong APEX activity, APEX2 exhibits strong in vitro 3′-phosphodiesterase and 3′-5′ exonuclease activities (*44*). We therefore examined the contribution of APEX1 or APEX2 to PARylation and ssDNA gap formation during 5hmdU elimination. Similar to SMUG1 loss, APEX1 knockdown had hardly any effect on nuclear PARylation in untreated cells (Fig. 3A). However, 5hmdC-dependent nuclear PARylation in total or EdU^{+} *Fancd2*$^{-/-}$ cells significantly decreased to near–wild-type levels (Fig. 3A and fig. S2C). APEX1 loss significantly suppressed spontaneous and 5hmdC-induced EdU-PAR foci in *Fancd2*$^{-/-}$ cells to wild-type levels (Fig. 3B). Moreover, loss of APEX1 significantly reduced 5hmdC-induced SSBs observed in *Fancd2*$^{-/-}$ cells to almost untreated levels (Fig. 3C). These data suggest that APEX1 is the main endonuclease responsible for most 5hmdC-induced SSBs in *Fancd2*$^{-/-}$ and, to a lesser extent, in wild-type cells. APEX1 depletion also substantially suppressed 5hmdC-mediated *Fancd2*$^{-/-}$ replication fork impairment and cell lethality (Fig. 3, D and E), indicating that APEX1-dependent SSBs account for the replication fork defects and lethality observed in 5hmdC-treated *Fancd2*$^{-/-}$ cells. As APEX1 knockdown does not fully restore cell viability or fork dynamics, these results also suggest that APEX1 may play additional roles during stability or resumption of replication forks. Similar to APEX1 depletion, APEX2 knockdown also reduced 5hmdC-mediated nuclear PARylation in total or S-phase (EdU^{+}) *Fancd2*$^{-/-}$ cells populations (fig. S4, A and B), to a lesser extent, than APEX1 depletion. APEX1 and APEX2 codepleted S-phase *Fancd2*$^{-/-}$ cells showed 5hmdC-induced PAR levels similar to those observed in APEX1-depleted 5hmdC-treated *Fancd2*$^{-/-}$ cells, indicating an epistatic relationship between APEX1 and APEX2. Moreover, APEX1 or APEX2 knockdown completely suppressed 5hmdC-induced EdU-PAR foci and SSBs (Fig. 3F and fig. S4C). These data indicate that APEX1, in combination with APEX2, is responsible for the increased PARylation and SSBs associated with nascent strand during 5hmdU removal. Consistent with this notion, APEX1 and APEX2 showed an epistatic relationship on PAR levels and lethality observed in 5hmdC-treated *Fancd2*$^{-/-}$ cells (Fig. 3E). These data point out to a concerted function of APEX1 and APEX2 at processing 5hmdU-derived AP sites, likely generating ssDNA gaps.

5hmdU-derived ssDNA gap persistence at replication forks exacerbates genomic instability and lethality in HRD cells

In unperturbed S-phase, ssDNA gap persistence due to inefficient Okazaki fragment ligation is signaled by PARP1-dependent PARylation, followed by XRCC1-mediated PARP1 eviction, to promote faithful gap repair (*45*). We reasoned that defective 5hmdC-dependent ssDNA gap processing either by excessive PARP1 retention or by PARP1 or XRCC1 loss would exacerbate ssDNA gap persistence and cell lethality, thus mimicking persistent unligated Okazaki fragments. XRCC1 knockdown increased further nuclear PARylation in 5hmdC-treated total or EdU^{+} *Fancd2*$^{-/-}$ cell populations while remaining unaffected in wild-type cells (Fig. 4A and fig. S2D). Likewise, the SIRF assay revealed a significant increase in EdU-PAR foci in 5hmdC-treated *Fancd2*$^{-/-}$ cells upon XRCC1 depletion (Fig. 4B). PARP1 or XRCC1 depletion further exacerbated 5hmdC-mediated *Fancd2*$^{-/-}$ cell lethality (Fig. 4C) similar to PARP1 trapping by olaparib (*25*) as a result of inefficient repair of ssDNA gaps. However, XRCC1 depletion did not further affect 5hmdC-mediated *Fancd2*$^{-/-}$ replication fork impairment (Fig. 4D). These data indicate that ssDNA gaps associated with replication forks in the absence of FANCD2 persist or accumulate to a larger extent upon XRCC1 loss.

Replication forks stalled by bulky base adducts stimulate postreplicative SCEs in an ssDNA gap– and PRIMPOL-dependent fashion (*14*). We therefore examined SCEs induced by 5hmdC-mediated ssDNA gaps in nascent DNA by exposing cells to 5hmdC for less than one cell cycle length (≈12 hours). We found that 5hmdC triggered a significant increase in SCEs in *Fancd2*$^{-/-}$ cells compared to untreated cells (Fig. 4E). Moreover, SMUG1 or APEX1 depletion suppressed 5hmdC-induced SCEs, while PARP1 or XRCC1 knockdown exacerbated them (Fig. 4E). These data indicate that 5hmdC-mediated ssDNA gaps in nascent strands occurring during the current cell cycle are a source of SCEs in HRD cells. Our findings suggest that defective repair of persistent replicative 5hmdC-induced ssDNA gaps accounts for increased PARylation, replication fork impairment, heightened SCEs, and lethality observed in *Fancd2*$^{-/-}$ cells.

HMCES-DPCs are responsible for 5hmdC-mediated ssDNA gaps in HRD cells

AP sites and other intermediate DNA ends during BER hamper replication fork progression, causing BRCs (*28*, *29*, *36*, *46*). AP sites are protected by HMCES to avoid cytotoxic DSB formation at the replication fork while promoting TLS bypass mechanisms (*35*, *36*, *40*). We therefore reasoned that HMCES could react to 5hmdU-derived AP sites arising during 5hmdC treatment. Upon preextraction, we observed a significantly higher proportion of nuclei stained positive for chromatin-bound Flag-tagged HMCES in *Fancd2*$^{-/-}$ than in wild-type cells under untreated conditions (Fig. 5A). *Fancd2*$^{-/-}$ cells also displayed a brighter chromatin-bound HMCES signal compared to its wild-type counterpart under spontaneous, methyl methanesulfonate (MMS) used as a positive control, or 5hmdC exposure (Fig. 5B). Moreover, chromatin-bound HMCES levels directly correlated with nascent strand 5hmdC misincorporation in a dose-dependent manner, reaching significantly higher levels in *Fancd2*$^{-/-}$ than in wild-type cells (Fig. 5B). We also confirmed these findings by cellular subfractionation and by rapid approach to DNA adduct recovery (RADAR) assays, showing a 5hmdC dose-dependent HMCES chromatin retention (fig. S5, A and B). These data suggest that *Fancd2*$^{-/-}$ cells present higher levels of endogenous AP site–bound HMCES than wild-type cells, which increase upon 5hmdC treatment in a dose-dependent manner. We next examined the chromatin retention activity of cell lines overexpressing either Cys^{2}→Ala (C2A) or Arg^{212}→Glu (R212E), two mutant versions of HMCES showing defective DPC formation and ssDNA binding activities, respectively. Consistent with their reported in vitro biochemical activities (*35*), HMCES-C2A showed impaired chromatin recruitment upon 5hmdC or MMS exposure, while HMCES-R212E completely

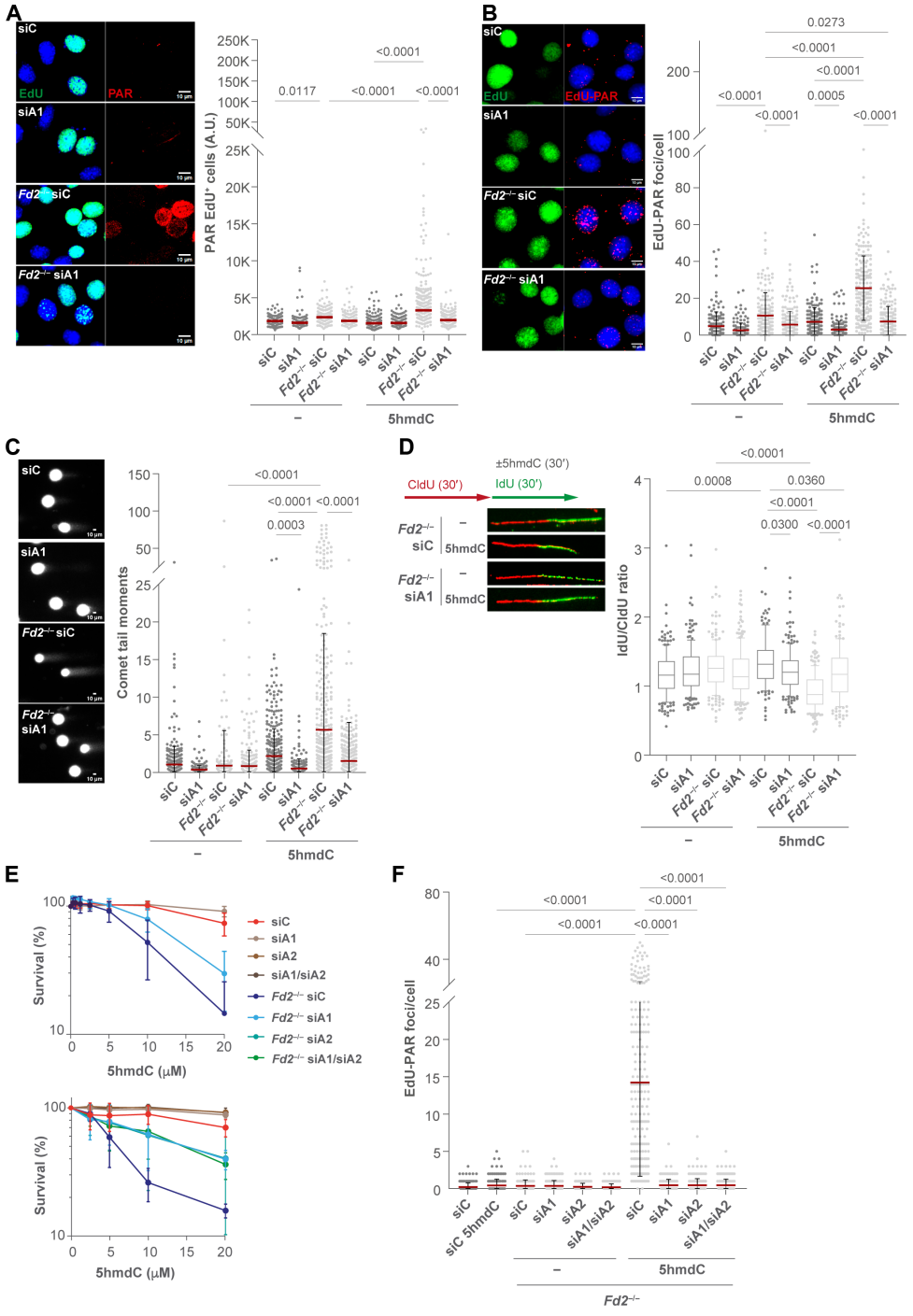

Fig. 3. APEX1 and APEX2 contribute to 5hmdC-induced ssDNA gap generation in HRD cells. (**A**) Left: Representative PAR (red) immunofluorescence images of siA1-depleted (siA1) wild-type or *Fancd2*$^{-/-}$ cells exposed to 5hmdC (10 μM) for 3 hours. DAPI (blue) stains nuclear DNA and EdU (green) stains S-phase cells. Right: Plot depicting PAR mean intensity signal per EdU^{+} nucleus. (**B**) Left: Representative images of EdU-PAR foci (red) by SIRF assay from wild-type, siA1 *Fancd2*$^{-/-}$, or *Fancd2*$^{-/-}$ siA1 cells exposed to 5hmdC (10 μM) for 3 hours. DAPI (blue) stains nuclear DNA and EdU (green) stains S-phase cells. Right: Plot depicting EdU-PAR foci per nucleus. (**C**) Left: Representative images of alkaline comet assay of APEX1 knockdown wild-type or *Fancd2*$^{-/-}$ cells exposed to 5hmdC (10 μM) for 3 hours. Right: Plot depicting comet tail moment per cell. (**D**) Top left: Scheme of DNA fiber assay. Bottom left: Representative images of DNA fibers from *Fancd2*$^{-/-}$ and *Fancd2*$^{-/-}$ siA1 cells untreated or exposed to 5hmdC (40 μM) for 30 min. Right: Box plot of the frequency of IdU/CldU ratio of siA1-depleted wild-type or *Fancd2*$^{-/-}$ cells upon 5hmdC treatment ($n = 200$ of each of the two biological replicates). (**E**) Top: MTT cell proliferation assay of siA1-depleted wild-type or *Fancd2*$^{-/-}$ cells exposed to the indicated dose of 5hmdC for 3 days ($n = 9$; means ± SD). Bottom: MTT cell proliferation assay of APEX1- or siA2-depleted wild-type or *Fancd2*$^{-/-}$ cells exposed to the indicated dose of 5hmdC for 3 days. (**F**) Plot depicting EdU-PAR foci per nucleus by SIRF assay from wild-type, *Fancd2*$^{-/-}$, siA1, siA2, *Fancd2*$^{-/-}$ siA1, and *Fancd2*$^{-/-}$ siA2 cells exposed to 5hmdC (10 μM) for 3 hours ($n = 2$).

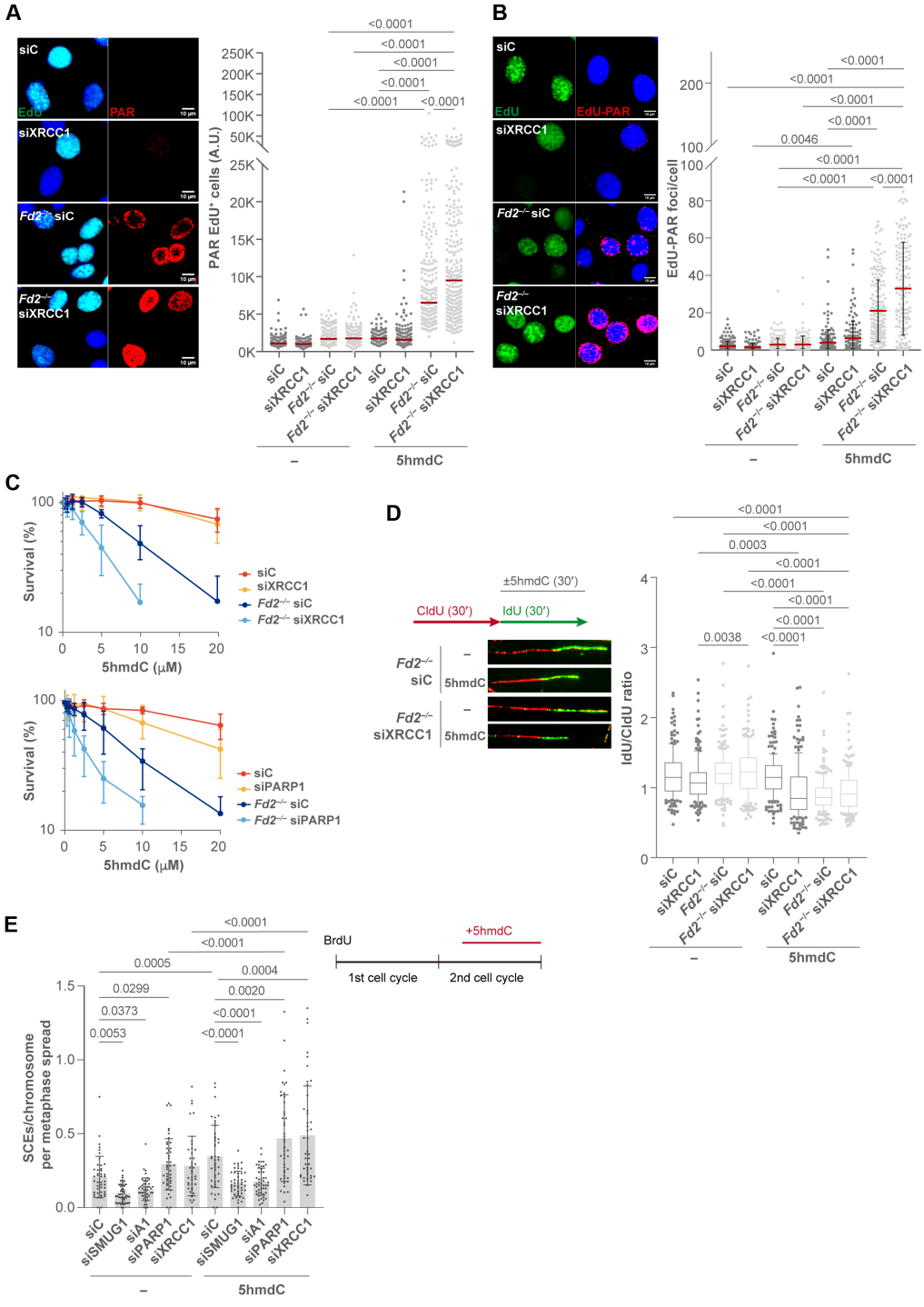

Fig. 4. XRCC1 depletion exacerbates 5hmdC-induced genomic instability and lethality of HRD cells. (**A**) Left: Representative PAR (red) immunofluorescence images of XRCC1-depleted wild-type or *Fancd2*$^{-/-}$ cells exposed to 5hmdC (10 μM) for 3 hours. DAPI (blue) stains nuclear DNA and EdU (green) stains S-phase cells. Right: Plot depicting PAR mean intensity signal per nucleus. (**B**) Left: Representative images of EdU-PAR foci (red) by SIRF assay of XRCC1-depleted wild-type or *Fancd2*$^{-/-}$ cells exposed to 5hmdC (10 μM) for 3 hours. DAPI (blue) stains nuclear DNA and EdU (green) stains S-phase cells. Right: Plot depicting EdU-PAR foci per nucleus. (**C**) Top: MTT cell proliferation assay of wild-type or *Fancd2*$^{-/-}$ cells lacking XRCC1 exposed to the indicated dose of 5hmdC for 3 days (n = 9; means ± SD). Bottom: MTT cell proliferation assay of wild-type, siPARP1, *Fancd2*$^{-/-}$, and *Fancd2*$^{-/-}$ siPARP1 cells exposed to the indicated dose of 5hmdC for 3 days (n = 5; means ± SD). (**D**) Top left: Scheme of DNA fiber assay. Bottom left: Representative images of DNA fibers from *Fancd2*$^{-/-}$ and *Fancd2*$^{-/-}$ siXRCC1 cells untreated or exposed to 5hmdC (40 μM) for 30 min. Right: Box plot of the frequency of IdU/CldU ratio of XRCC1-depleted wild-type or *Fancd2*$^{-/-}$ cells upon 5hmdC treatment (n = 200 of each of the two biological replicates). (**E**) Top right: Scheme of the SCE assay. Left: Bar plot of SCE/chromosome per metaphase from SMUG1-, APEX1-, XRCC1-, or PARP1-depleted *Fancd2*$^{-/-}$ cells exposed to 5hmdC (10 μM) for 12 hours (n = 50 of each of the two biological replicates; bar represents means ± SD).

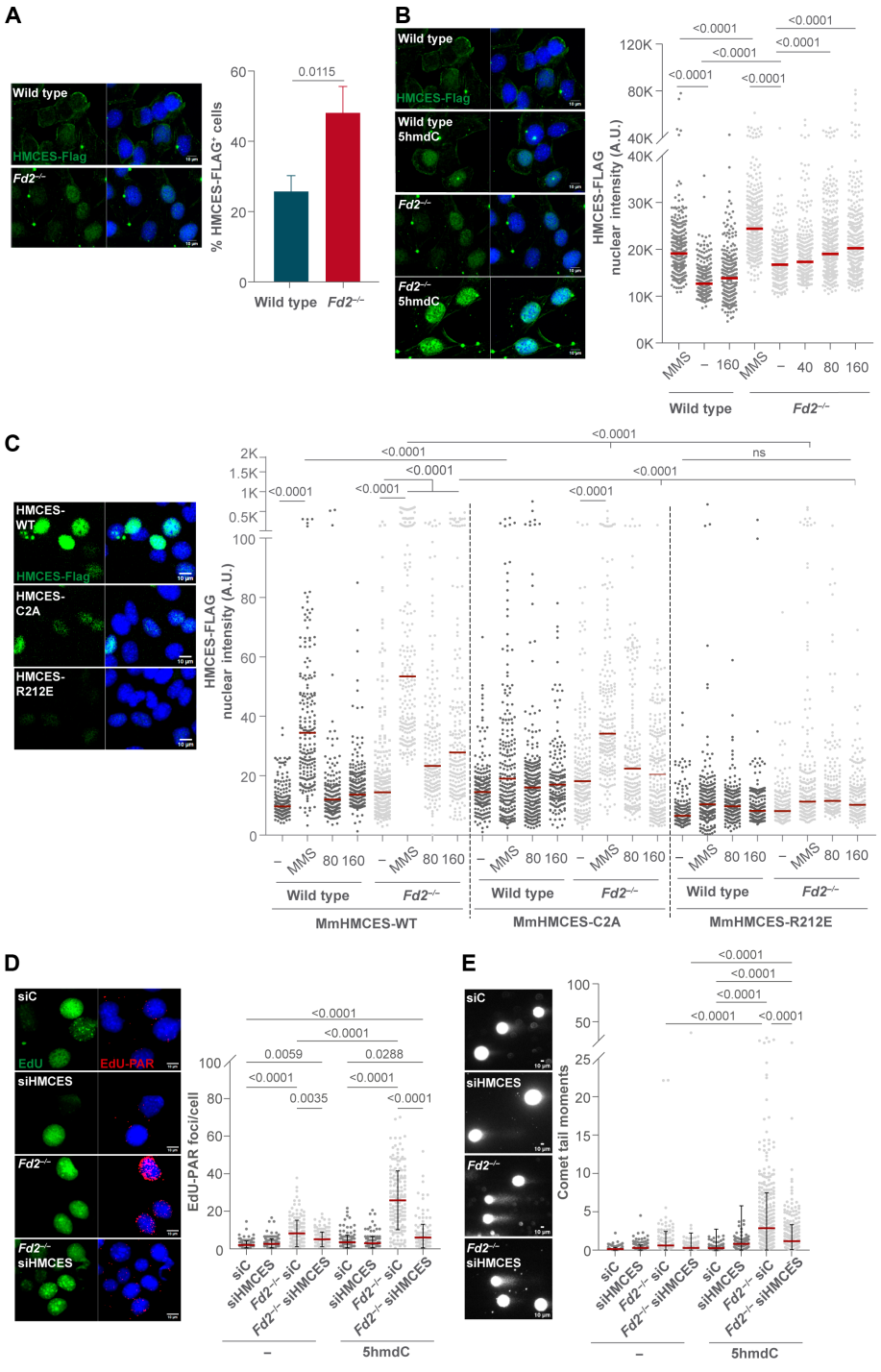

Fig. 5. HMCES accumulates in nuclei and is responsible for 5hmdC-mediated genomic instability observed in HRD cells. (**A**) Left: Representative immunofluorescence images of Flag-tagged HMCES (green) positive nuclei from wild-type or *Fancd2*$^{-/-}$ cells. Right: Percentage of HMCES-FLAG^{+} wild-type and *Fancd2*$^{-/-}$ cells. (**B**) Left: Representative immunofluorescence images of HMCES positive nuclei from wild-type or *Fancd2*$^{-/-}$ cells upon combined 5hmdC (160 μM) and *N*-carbobenzyloxy-L-leucyl-L-leucyl-L-leucinal (MG132; 10 μM) treatments for 3 hours. Right: HMCES-FLAG mean intensity signal per nucleus from wild-type and *Fancd2*$^{-/-}$ cells upon 5hmdC (3 hours) or MMS (0.5 mM, 30 min). Treatments were combined with MG132 (10 μM). (**C**) Left: Images of FLAG-tagged HMCES positive nuclei from *Fancd2*$^{-/-}$ cells, expressing MmHMCES-WT-FLAG, MmHMCES-C2A-FLAG, or MmHMCES-R212E-FLAG upon 5hmdC exposure (160 μM, 3 hours). Right: Plot depicting HMCES-FLAG mean intensity signal per nucleus from wild-type or *Fancd2*$^{-/-}$ cells expressing MmHMCES-WT-FLAG, MmHMCES-C2A-FLAG, or MmHMCES-R212E-FLAG upon 5hmdC (indicated dose for 3 hours) or MMS (0.5 mM). Treatments were combined with MG132 (10 μM). ns, not significant. (**D**) Left: Representative images of EdU-PAR foci by SIRF assay from HMCES-depleted wild-type or *Fancd2*$^{-/-}$ cells exposed to 5hmdC (10 μM) for 3 hours. DAPI (blue) stains nuclear DNA and EdU (green) stains S-phase cells. Right: Plot depicting EdU-PAR foci per nucleus. (**E**) Left: Representative images of alkaline comet assay from HMCES-depleted wild-type or *Fancd2*$^{-/-}$ cells following 5hmdC treatment (10 μM) for 3 hours. Right: Plot depicting comet tail moment per cell.

abolished it (Fig. 5C and fig. S6). These data suggest that 5hmdU-derived AP sites on nascent DNA strand are recognized by HMCES, forming HMCES-DPCs. We predicted that HMCES loss would increase cytotoxic ssDNA gaps on nascent DNA strand by APEX1-mediated incision of AP sites right at or behind the fork, resulting in a synthetic lethal phenotype in HRD cells. To our surprise, HMCES knockdown markedly decreased 5hmdC-induced nuclear PARylation in total or EdU$^+$ *Fancd2*$^{-/-}$ cell populations (fig. S7, A and B), EdU-PAR foci in S-phase cells (Fig. 5D), and SSBs observed in *Fancd2*$^{-/-}$ cells (Fig. 5E), suggesting that HMCES-DPCs on nascent DNA strand are responsible for a large subset of 5hmdC-induced ssDNA gaps observed in *Fancd2*$^{-/-}$ cells. Consistent with the protective role of HMCES during replication (*35*), HMCES depletion increased nuclear γ-H2AX, which was further elevated in the absence of FANCD2 (fig. S7C). Nevertheless, γ-H2AX levels remained relatively unchanged during 3 hours of 5hmdC treatment, suggesting that ssDNA gaps in nascent DNA arising from AP sites unprotection due to HMCES loss do not result in cumulative DSBs (fig. S7C). HMCES depletion also restored *Fancd2*$^{-/-}$ replication fork progression and symmetry to wild-type levels (Fig. 6, A and B). 5hmdC-induced heightened chromosomal aberrations were markedly reduced upon HMCES depletion (Fig. 6C), specifically those of radial chromosomes, which arose at the expense of chromosomal gaps (fig. S8). As a consequence, 5hmdC-induced HRD cell viability was also notably improved upon HMCES depletion (Fig. 6D), indicating that HMCES-DPCs formed at BER intermediates are responsible for replication fork impairment, chromosomal instability, and cell lethality in HRD cells. To rule out that the phenotypic suppression by HMCES knockdown was a consequence of pooled small interfering RNA (siRNA) off-targets, we validated our results using four independent siRNAs against HMCES (from number 1 to number 4) compared to pooled siRNAs, obtaining similar results to pooled siRNAs (fig. S9). We also validated our results using human BRCA2–deficient DLD-1 cells, which were previously reported to be sensitive to 5hmdU (*25*). HMCES knockdown also suppressed 5hmdC-mediated BRCA2$^{-/-}$ cell lethality (Fig. 6E), thus broadening these findings to different human genetic backgrounds. To directly examine the effects of HMCES depletion on DNA replication intermediates, we use DNA electron microscopy (EM) to monitor the frequency of broken replication fork intermediates, possibly resulting from ssDNA gap breakage (*47*). In agreement with our genetic data, compared to untreated condition, 5hmdC-treated *Fancd2*$^{-/-}$ cells displayed significant increase in DNA replication intermediates with asymmetric branches, indicating broken forks, possibly resulting from the processing of ssDNA gaps present in *Fancd2*$^{-/-}$ cells (Fig. 6F and fig. S10) (*47*). HMCES depletion largely suppressed 5hmdC-mediated fork instability and ssDNA gap accumulation (Fig. 6F). We also attempted to validate these findings by S1 nuclease DNA fiber assay but failed to obtain reproducible results in MEFs. To overcome this, we knocked out FANCD2, HMCES, or both genes in human RPE-1 cells by CRISPR-Cas9 approaches (fig. S11, A and B). Consistent with published data, HMCES loss did not affect unperturbed replication fork progression (*40*) or the amount of ssDNA gaps, suggesting that unprotection of spontaneous AP sites upon HMCES loss does not affect overall levels of ssDNA gaps (fig. S11C). Despite S1 insensitivity in untreated *FANCD2*$^{-/-}$ RPE-1 cells, small ssDNA gaps were visible in all *Fancd2*$^{-/-}$ MEFs samples by EM (Fig. 6F and fig. S10), compatibly with AP site accumulation on template strands. Moreover, exposure of *FANCD2*$^{-/-}$ RPE-1 cells to 5hmdC (10 μM) significantly affected 5′-iododeoxyuridine (IdU) track length, suggesting that FANCD2 is required to avoid ssDNA gap formation. Notably, HMCES depletion suppressed 5hmdC-induced ssDNA gap formation in *FANCD2*$^{-/-}$ cells detected by S1 nuclease (fig. S11C), confirming that HMCES-DPCs are responsible for 5hmdU-derived ssDNA gap accumulation in HRD cells. We also found that low expression levels of HMCES correlated with lower overall survival in two independent cohorts of patients with breast adenocarcinoma, one from TCGA (1089 patients) and another from a set of curated breast cancer cohorts from GEO (2976 patients) (Fig. 6G and fig. S11D). These data suggest that HMCES loss might play a role in breast cancer aggressiveness or patient outcome, although these findings need further validation.

HMCES-DPCs on template DNA strand showed an epistatic relationship over APEX1 incision to avoid toxic DSB formation (*34*, *35*). We therefore examined nuclear PARylation and viability phenotypes upon depletion of HMCES, APEX1, APEX2, or their combinations. Nuclear PARylation in HMCES APEX1 double-knockdown EdU$^+$ cells resembled the one seen in APEX1 knockdown *Fancd2*$^{-/-}$ cells (Fig. 7A). However, PARylation in HMCES APEX2 double-knockdown *Fancd2*$^{-/-}$ cells resembled the one observed in *Fancd2*$^{-/-}$ HMCES single-knockdown EdU$^+$ cells (Fig. 7B). Moreover, knockdown of HMCES, APEX1, or APEX2 also showed an epistatic suppressive phenotype on *Fancd2*$^{-/-}$ cell survival (Fig. 7, C and D). These data suggest that HMCES, APEX1, and APEX2 function in the same genetic pathway during the processing of 5hmdU from nascent DNA.

PRIMPOL mediates a subset of 5hmdC-mediated ssDNA gaps

Replication fork stalling by bulky base adducts generates postreplicative ssDNA gaps throughout the primase and polymerase activities of PRIMPOL (*14*, *19*). We therefore examined the contribution of PRIMPOL to 5hmdC-induced ssDNA gap formation in our cell lines. PRIMPOL depletion had little effect on PARylation levels in untreated EdU$^+$ *Fancd2*$^{-/-}$ cells. Nevertheless, PRIMPOL knockdown largely suppressed 5hmdC-mediated PARylation, not reaching wild-type levels (fig. S12). In addition, PRIMPOL depletion partially suppressed 5hmdC-induced EdU-PAR SIRF foci in *Fancd2*$^{-/-}$ cells (Fig. 8A). Moreover, PRIMPOL depletion significantly reduced 5hmdC-induced ssDNA gaps in *Fancd2*$^{-/-}$ cells, but not reaching levels seen in the untreated condition (Fig. 8B). These data suggest that a proportion of 5hmdC-induced ssDNA gaps depends on PRIMPOL. This situation contrasted to APEX1-depleted cells, whereby APEX1 depletion completely abolished 5hmdC-induced ssDNA gaps in both backgrounds. These data indicate that, in addition to PRIMPOL-mediated ssDNA gaps, 5hmdC induces other types of ssDNA gaps, probably arising from unrepaired APEX1-mediated SSBs. Consistent with this, PRIMPOL partially accounted for the 5hmdC-induced lethality observed in *Fancd2*$^{-/-}$ cells (Fig. 8C). APEX1 PRIMPOL or HMCES PRIMPOL double-knockdown cells displayed the same viability as single PRIMPOL–depleted *Fancd2*$^{-/-}$ cells (Fig. 8C). These data suggest that a subset of ssDNA gaps arising from cytotoxic HMCES-DPCs is PRIMPOL dependent, whereas others are independently formed. We also examined the contribution of HMCES-DPCs on nascent DNA to 5hmdC-dependent SCEs. As previously reported for bulky adducts on template DNA strands (*14*), PRIMPOL depletion efficiently suppressed heightened 5hmdC-dependent SCEs observed in *Fancd2*$^{-/-}$ cells. Moreover, HMCES loss also blunted this response, and codepletion

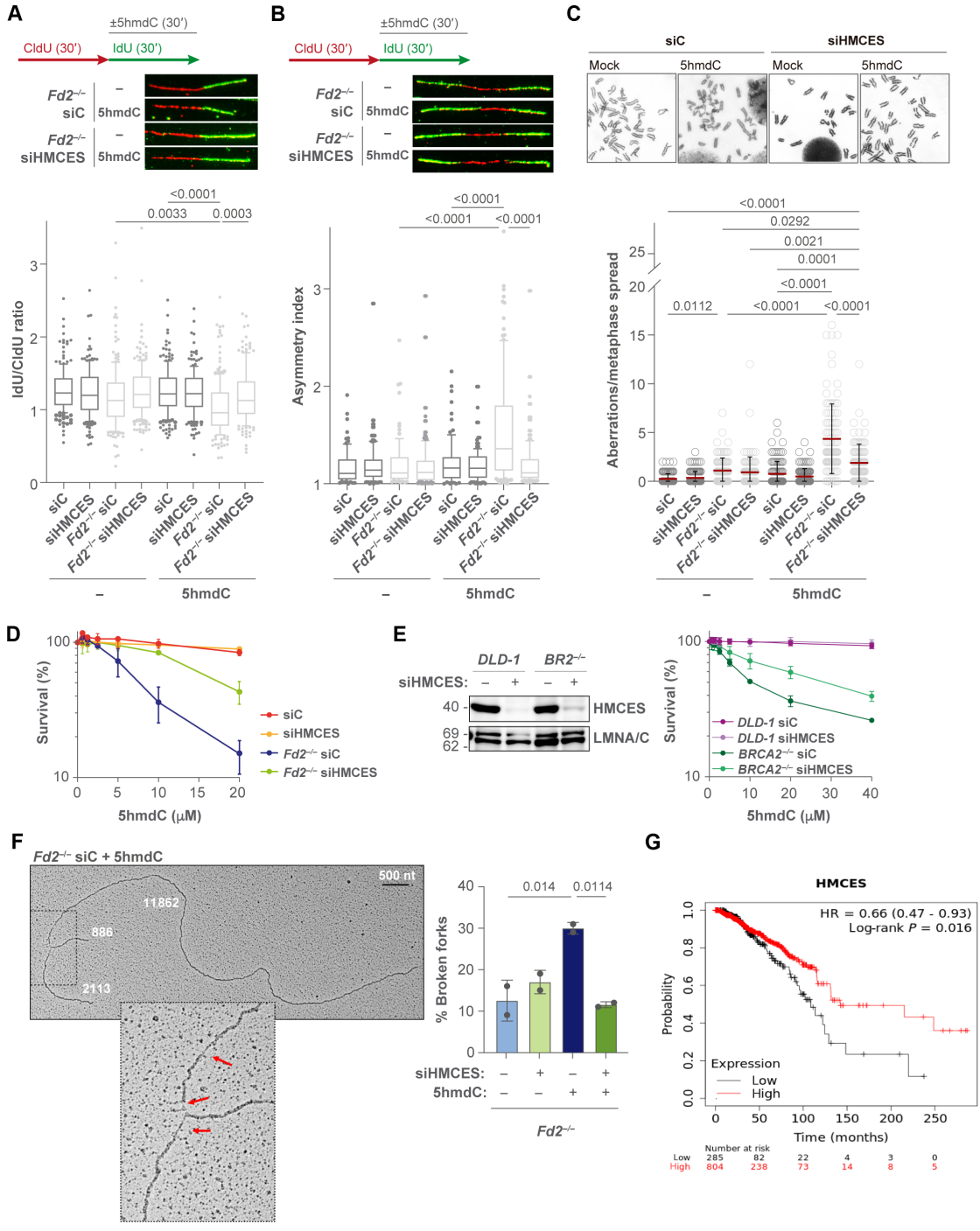

Fig. 6. HMCES depletion rescues 5hmdC-induced replication fork defects and ssDNA gap accumulation in HRD cells. (**A**) Top: Scheme of DNA fiber assay and representative images of DNA fibers from *Fancd2*$^{-/-}$ and *Fancd2*$^{-/-}$ siHMCES cells untreated or exposed to 5hmdC (40 μM, 30 min). Bottom: Box plot of the frequency of IdU/CldU ratios of HMCES-deficient wild-type or *Fancd2*$^{-/-}$ cells upon 5hmdC treatment ($n = 200$). (**B**) Top: Scheme of DNA fiber assay and representative images of bidirectional fibers from *Fancd2*$^{-/-}$ and *Fancd2*$^{-/-}$ siHMCES cells untreated or exposed to 5hmdC (40 μM, 30 min). Bottom: DNA fiber asymmetry index from HMCES-depleted wild-type or *Fancd2*$^{-/-}$ cells upon 5hmdC treatment. (**C**) Top: Chromosome aberrations from HMCES knockdown *Fancd2*$^{-/-}$ cells following 5hmdC treatment (10 μM, 40 hours). Bottom: Plot depicting chromosome aberrations/metaphase spread ($n = 50$ of each of the two biological replicates; bar represents means ± SD). (**D**) MTT cell proliferation assay of HMCES-depleted wild-type or *Fancd2*$^{-/-}$ cells exposed to the indicated dose of 5hmdC for 3 days ($n = 5$; means ± SD). (**E**) Left: HMCES protein depletion examined by Western blots of *DLD-1* or *BRCA2*$^{-/-}$ cells extracts. Right: MTT cell proliferation assay of HMCES-deficient wild-type and *BRCA2*$^{-/-}$ cells exposed to the indicated dose of 5hmdC for 6 days ($n = 6$; means ± SD). (**F**) Left: Representative EM image of a broken replication fork from 5hmdC-exposed *Fancd2*$^{-/-}$ cells (10 μM, 3 hours). Rectangle shows fork junction magnification. Red arrows indicate ssDNA gaps. Right: Percentage of broken forks in HMCES-knocked down (KD) *Fancd2*$^{-/-}$ cells following 5hmdC treatment. A total of 100 forks were scored for each condition ($n = 2$). (**G**) Overall survival plot of breast cancer cohort of the TCGA repository.

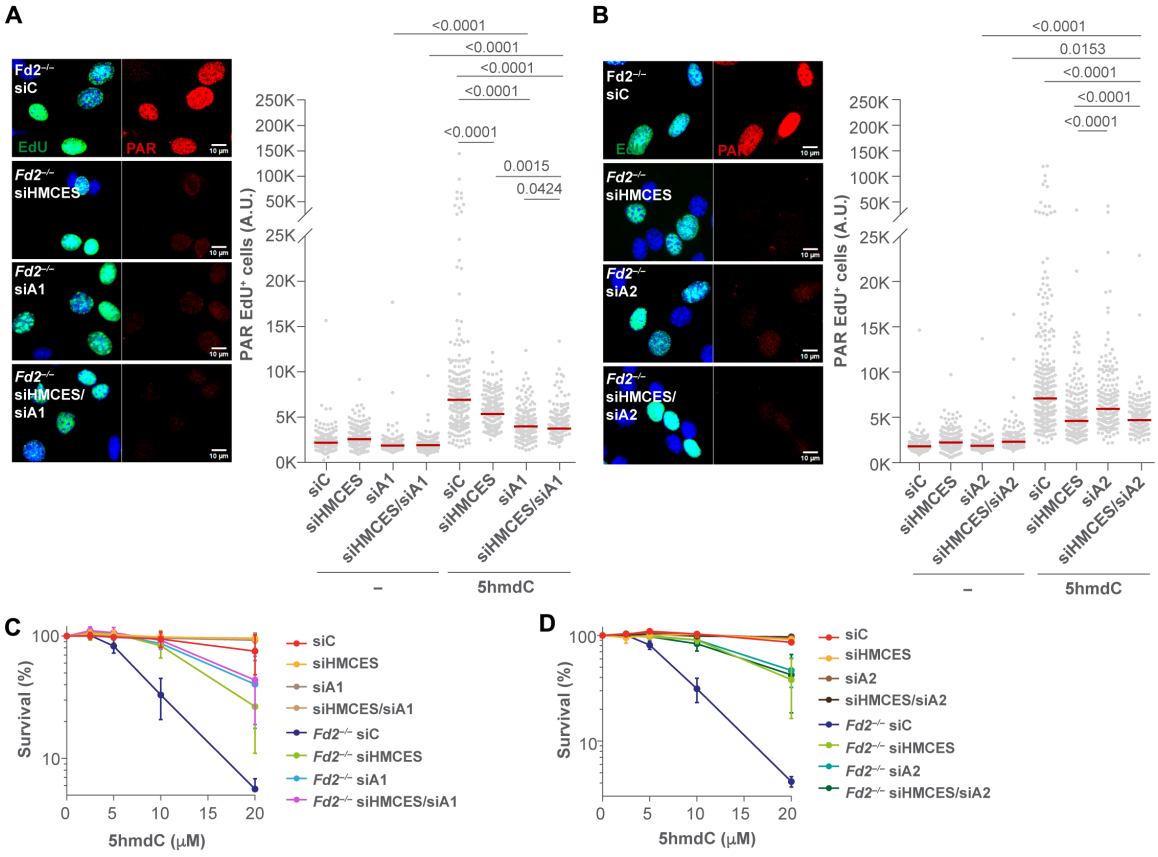

Fig. 7. HMCES, APEX1, and APEX2 function in a common BER genetic pathway during 5hmdU removal. (**A**) Left: Representative PAR (red) immunofluorescence images from *Fancd2*$^{-/-}$ cells upon depletion of HMCES, APEX1, or their combinations exposed to 5hmdC (10 μM, 3 hours). DAPI (blue) stains nuclear DNA and EdU (green) stains S-phase nuclei. Right: Plot depicting PAR mean intensity signal per nucleus. (**B**) Left: Representative PAR (red) immunofluorescence images from *Fancd2*$^{-/-}$ cells upon depletion of HMCES, APEX2, or their combinations exposed to 5hmdC (10 μM, 3 hours). DAPI (blue) stains nuclear DNA and EdU (green) stains S-phase cells. Right: Plot depicting PAR mean intensity signal per nucleus. (**C**) MTT cell proliferation assay of HMCES-, APEX1-, or HMCES siA1–depleted wild-type or *Fancd2*$^{-/-}$ cells exposed to the indicated dose of 5hmdC for 3 days ($n = 5$; means ± SD). (**D**) MTT cell proliferation assay of HMCES-, APEX2-, or HMCES siA2–depleted wild-type or *Fancd2*$^{-/-}$ cells exposed to the indicated dose of 5hmdC for 3 days.

of HMCES and PRIMPOL showed an epistatic phenotype (Fig. 8D). These data indicate that 5hmdC-induced HMCES-DPCs in nascent DNA trigger the formation of PRIMPOL-dependent ssDNA gaps during the ongoing cell cycle (Fig. 8E). HMCES-DPC–dependent ssDNA gaps are, therefore, responsible for heightened SCEs and suggest a more complex role of HMCES in protecting AP sites than previously anticipated.

DISCUSSION

Recent work has identified the molecular mechanisms of dU, 5CldU, or 5hmdU genotoxicity (*25*–*29*). During dU, 5CldU, or 5hmdU misincorporation, *N*-glycosylase activity of uracil-DNA glycosylase (UNG1/2) or SMUG1 mediates efficient excision of dU, 5CldU, or 5hmdU. When misrepaired, UNG- or SMUG1-mediated AP sites trigger BRCs due to persistent BER intermediates in template DNA (*25*–*29*). In the absence of AP site generation, unprocessed dU also triggers an ATR-dependent response characterized by replication fork slowing and PRIMPOL-dependent ssDNA gap formation, presumably as a consequence of replication fork stalling (*29*). Our study complements the previous ones by reporting that HMCES-DPCs, generated upon 5hmdU misincorporation on the nascent strand, are an additional toxic BER intermediate that challenges replication fork dynamics. By combining different cellular and genetic approaches, we conclude that HMCES-DPCs on nascent DNA promote accumulation of postreplicative ssDNA gaps, likely responsible for replication forks stalling. Our study identifies two sources of ssDNA gaps. One arises from direct incisions at the HMCES-DPC by APEX1/APEX2, which probably accounts for small ssDNA gaps at or behind the fork. The second one is dependent on both APEX1 and PRIMPOL activities, which probably accounts for long ssDNA gaps, due to PRIMPOL-mediated repriming of DNA synthesis to accomplish genome duplication. Recent reports show that HMCES binds to uracil-DNA glycosylase (UDG)-mediated AP sites in ssDNA to inhibit APEX1 incision in in vitro assays, while the self-reversal activity releases HMCES from double-stranded DNA (*35*, *37*, *38*). *Fancd2*$^{-/-}$ cells displayed high chromatin levels of HMCES, which are dependent on its DNA binding and cross-linking activities (*35*). Therefore, HMCES-DPCs might function as a second protection tier to AP sites embedded on ssDNA stretches, in addition to FA/BRCA2-dependent RAD51 AP site protection from MRE11 incision (*47*). In our working model (Fig. 8E), misincorporation of multiple 5hmdU on nascent DNA is processed by the concerted functions of SMUG1, followed by APEX1/2 in a staggered fashion. Initial nicks of multiple

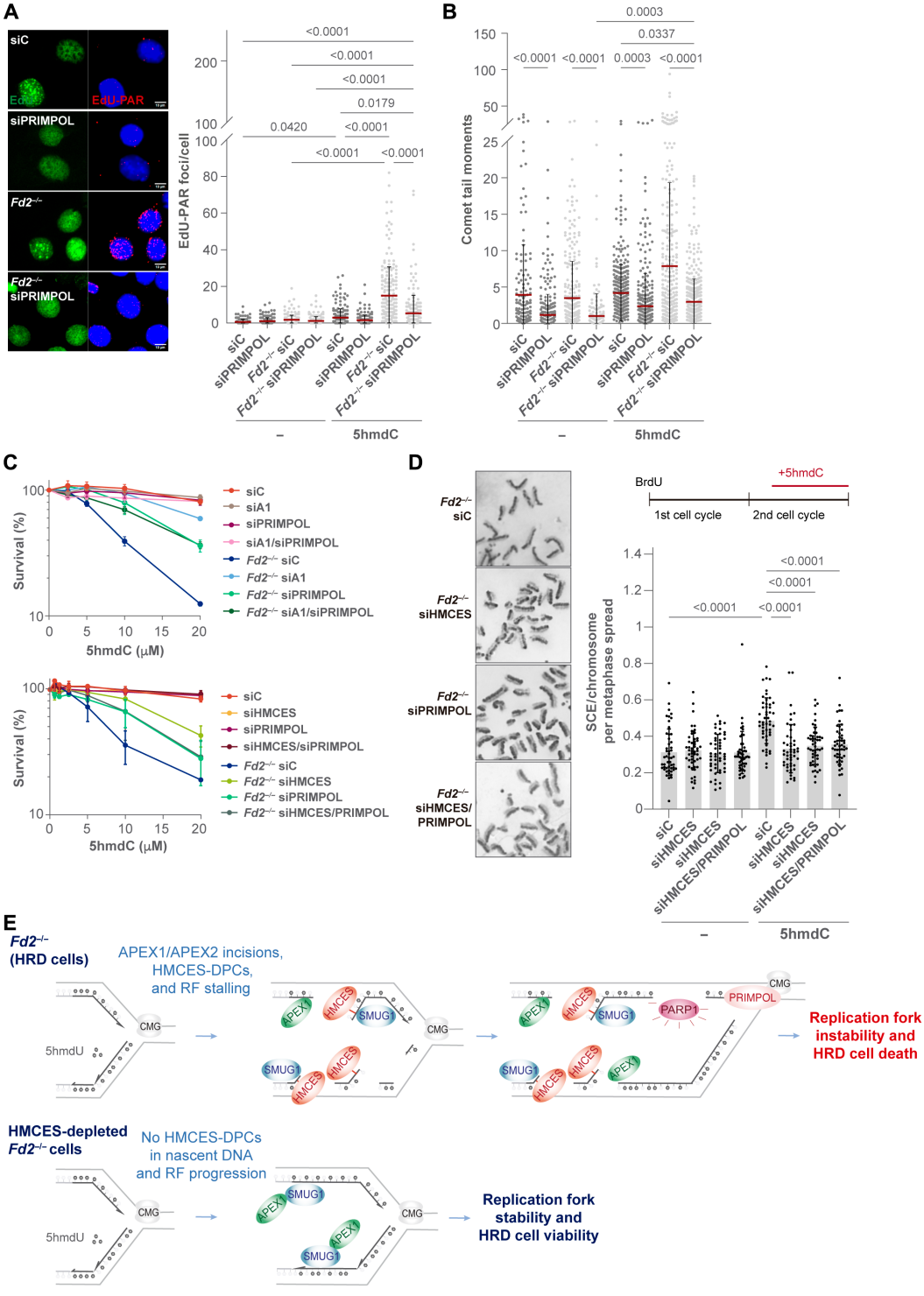

Fig. 8. HMCES is responsible for PRIMPOL-dependent ssDNA gap accumulation. (**A**) Left: Representative images of EdU-PAR foci (red) by SIRF assay from wild-type, siPRIMPOL, *Fancd2*$^{-/-}$, and *Fancd2*$^{-/-}$ siPRIMPOL cells exposed to 5hmdC (10 μM, 3 hours). DAPI (blue) stains nuclear DNA and EdU (green) stains S-phase cells. Right: Plot depicting EdU-PAR foci per nucleus. (**B**) Plot depicting comet tail moment per cell from PRIMPOL-depleted wild-type or *Fancd2*$^{-/-}$ cells following 5hmdC treatment (10 μM, 3 hours). (**C**) Top: MTT cell proliferation assay of wild-type or *Fancd2*$^{-/-}$ cells knocked down for APEX1, PRIMPOL, or APEX1 PRIMPOL and exposed to the indicated dose of 5hmdC for 3 days. Bottom: MTT cell proliferation assay of wild-type or *Fancd2*$^{-/-}$ cells knocked down for APEX1, PRIMPOL, or APEX1 PRIMPOL exposed to the indicated dose of 5hmdC for 3 days. (**D**) Left: Representative images of SCEs from *Fancd2*$^{-/-}$, *Fancd2*$^{-/-}$ siHMCES, *Fancd2*$^{-/-}$ siPRIMPOL, and *Fancd2*$^{-/-}$ siHMCES/siPRIMPOL cells exposed to 5hmdC (10 μM, 12 hours). Top right: Scheme of SCE assay. Bottom right: Bar plot of SCE/chromosome per metaphase spread ($n = 50$ of each of the two biological replicates; bar represents means ± SD). (**E**) Working model depicting the mechanism of replication fork instability by HMCES during the removal of 5hmdU in the absence of the replication fork maintenance FA pathway. RF, replication fork.

AP sites in nascent ssDNA would promote BER-mediated ssDNA flap exposure, in which HMCES efficiently binds to form HMCES-DPCs. By corrupting late steps of BER, HMCES-DPCs would impair replication fork progression in the absence of the FA/BRCA pathway. Defective RAD51 stabilization by the lack of FANCD2-FANCI nucleofilament formation would leave unprotected AP sites. Throughout its cross-linking activity, HMCES would shield toxic AP sites while avoiding APEX1-mediated SSBs, at the expense of impairing replication fork progression. In contrast to the reported self-reversal activity of HMCES on double-stranded DNA, HMCES in ssDNA may undergo FANCJ-mediated denaturation and subsequent proteasome or SPRTN-mediated proteolysis (*35*, *39*). This replication fork–associated HMCES degradation is predicted to leave a peptide bound to the ring-opened AP through a hard-to-degrade thiazolidine bond. In this situation, APEX1 efficiently incises 5′ to the DNA peptide cross-link through its phosphodiesterase activity (*48*–*51*). By physically interacting with APEX2, PCNA, and ATR, APEX1 would promote checkpoint activation while mediating nucleolytic processing of HMCES peptide (*48*–*51*). In agreement with this, loss of APEX1 or APEX2 suppressed 5hmdC-mediated *Fancd2*$^{-/-}$ EdU-PAR foci formation, SSB accumulation, and heightened SCEs. The fact that APEX2 depletion suppressed 5hmdC-induced SSBs to levels observed in APEX1 knockdown cells strongly suggests that APEX1 and APEX2 activities are genetically linked. As a result, persistent HMCES peptide cross-linked to 5′-DNA, or futile SSB ligation cycles mimicking unligated Okazaki fragments, would hinder replication fork progression, leading to HRD cell lethality.

A consequence of 5hmdU-induced stalled replication fork is the activation of DNA damage tolerance mechanisms in HRD cells (*17*, *19*, *27*, *33*). Whereas replication fork reversal has been demonstrated to promote fork degradation in HRD cells (*20*, *41*, *52*), template switching (TS) and PRIMPOL-mediated repriming are perhaps the chosen mechanisms to accomplish faithful DNA duplication while leaving cytotoxic ssDNA gaps behind replication forks (*33*). Our data point out a major role for PRIMPOL in a subset of 5hmdU-mediated ssDNA gaps. As previously observed by Piberger *et al.* (*14*), cumulative ssDNA gaps induced by bulky-adducted bases are repaired throughout a PRIMPOL-dependent TS mechanism, leading to increased SCEs. In agreement with their observations, AP site–derived HMCES-DPCs in nascent DNA also stimulated SCEs in HR-deficient *Fancd2*$^{-/-}$ cells. Heightened SCEs in *Fancd2*$^{-/-}$ cells were completely dependent on PRIMPOL and on HMCES, which showed an epistatic relationship, suggesting that most SCEs in HRD cells arise from PRIMPOL-dependent ssDNA gaps. Moreover, depletion of SMUG1 or APEX1 factors generating AP sites or incisions suppressed 5hmdC-mediated SCEs, whereas loss of the gap repair XRCC1 or PARP1 factors resulted in ssDNA gap persistence and SCE exacerbation. Together, these results suggest that HMCES-DPCs in nascent DNA induce PRIMPOL-dependent ssDNA gaps and SCEs. As *Fancd2*$^{-/-}$ cells are deficient in RAD51-mediated HR, it would be interesting to identify whether RAD51, RAD52, or other paralogues promote strand invasion and faithful SCEs completion in these cells. Our data analysis using two independent large breast tumor cohorts (TCGA and Győrffy repositories) establishes a correlation of decreased cell survival with low HMCES expression in breast cancer (*53*), where HRD tumors are overrepresented. This may suggest that loss of HMCES may contribute to disease progression or relapse, which could be a useful biomarker of HRD cancer susceptibility. More research addressing these aspects in preclinical and clinical setting is further needed.

We directly monitored replication fork instability in MEFs by EM. We found that HMCES-DPC persistence leads to broken forks in FANCD2-deficient MEFs, possibly due to nuclease access to abasic DNA templates in proximity of HMCES-DPC. We also detected small ssDNA gaps in all FANCD2-deficient MEFs, probably due to inefficient AP site quenching by RAD51, thus explaining the concomitant increased chromatin recruitment of HMCES. S1 fiber assays in human RPE-1 cell lines reproducibly confirmed a significant increase in ssDNA gaps in *FANCD2*$^{-/-}$ cells exposed to 5hmdC as a consequence of HMCES-DPCs, and HMCES loss largely suppressed 5hmdC-induced ssDNA gap accumulation upon S1 treatment. However, our S1 nuclease fiber assay was not sensitive enough to detect all ssDNA gaps identified by EM. One possible explanation is that most ssDNA gaps detected by S1 nuclease assay are large gaps, such as the ones generated by PRIMPOL activity. Probably, APEX1-mediated ssDNA gaps at 5′-DPC are shorter and require robust 3′-5′ exonuclease activity, such as the one catalyzed by APEX2, providing a substrate for PARP signaling. This second class of ssDNA gaps might also require further extension by long-range resection nucleases [DNA2 or Exonuclease 1 (EXO1)] as recently suggested by other laboratories (*54*, *55*) or harsher cell permeabilization (*47*) to allow S1 nuclease access. Our study uncovers the diverse nature of ssDNA gap formation in nascent DNA and highlights HMCES-DPCs as novel endogenous source, contributing to genomic instability with consequences beyond our expectations. Further work is needed to delineate their impact on tumorigenesis.

MATERIALS AND METHODS

Cell lines and reagents

Wild-type and *Fancd2*$^{-/-}$ MEFs and tumor protein p53 (*TP53*)$^{-/-}$ RPE-1 cells were grown in Dulbecco's modified Eagle's medium (Corning, Midland, MI, USA) supplemented with 10% fetal bovine serum and 1% penicillin/streptomycin (Gibco, Thermo Fisher Scientific, Waltham, MA, USA) in a 5% CO_2 incubator at 37°C. DLD-1, BRCA2$^{+/+}$, and BRCA2$^{-/-}$ cells were grown in RPMI 1640 (Biowest) supplemented with 2 mM glutamine, 10% fetal bovine serum, and 1% penicillin/streptomycin, and DLD-1 and BRCA2$^{-/-}$ were also grown with hygromycin B (0.1 mg/ml). Murine HMCES cDNA was purchased from Sino Biological Inc. (Beijing, China). HMCES-WT, HMCES-C2A, and HMCES-R212E constructs were generated by site-directed mutagenesis, using the following forward and reverse primers: HMCES-C2A mutation (5′-ATGGATCCACCATGGCCGGGCGAACGTCCT and 5′-AGGACGTTCGCCCGGCCATGGTGGATCCAT); HMCES-R212E mutation (5′-TGACATCCACAGCGAGATGCCTGCCATACT and 5′-AGTATGGCAGGCATCTCGCTGTGGATGTCA). The constructs were Bam HI–Not I adapted and subcloned in pCAG-BSR vector. pCAG-BSR plasmids harboring HMCES-C2A, HMCES-C2A, or HMCES-R212E were confirmed by Sanger sequencing. The plasmid was stably transfected into wild-type and *Fancd2*$^{-/-}$ MEFs and selected on growth medium containing BSR (4 μg/ml).

5hmdC (PY 7588, Berry & Associates, Dexter, MI, USA) was dissolved in phosphate-buffered saline (PBS; 10 mM stock concentration). 5-Bromo-2′-deoxyuridine (BrdU; B5002, Sigma-Aldrich, St. Louis,

MO, USA) was dissolved in PBS and added to cell cultures at 10 μM final concentration. 5-EdU (BCN-001-100, baseclick, Munich, Germany) and Biotin-PEG3-azide (BCFA-021-5, baseclick) were dissolved in dimethyl sulfoxide (DMSO; 10 mM stock concentration). CldU (Sigma-Aldrich, C6891) and IdU (Sigma-Aldrich, I7125) were dissolved in PBS (2′5 mM stock solution) and added to cell cultures to a final concentration of 20 and 200 μM, respectively. SIRF assay was developed by DUO92002, DUO92004, and DUO92007 according to the manufacturer's instructions (Sigma-Aldrich). *N*-carbobenzyloxy-L-leucyl-L-leucyl-L-leucinal (MG132) was dissolved in DMSO (10 mM; Sigma-Aldrich, 474790). siRNAs were purchased from the D'harmacon siGENOME siRNA pool (APEX1, M-042935-01; APEX2, M-050966-00; DCK, M-055649-01; DCTD, M-058063-02; murine HMCES, M-062972-00; human HMCES, M-020333-01; PARP1, M-040023-00; PRIMPOL, M-067173-00; SMUG1, M-041546-01; and XRCC1, M-046270-00). siRNAs were transfected for 24 hours using RNAiMAX (Invitrogen) according to the manufacturer's instructions. The antibodies used were against PAR (Millipore, MABE1016, Merck Millipore, Burlington, MA, USA), ERCC1 (sc-8408), PCNA (sc-56), Lamin A/C (sc-376248), BrdU (BU1/75, Abcam, Cambridge, England), IdU (Sigma-Aldrich, SAB3701448), Biotin (B7653, Sigma-Aldrich), HMCES (NPB2-14410, Novus Biologicals, Centennial, CO, USA), SMUG1 (E7P4I, Cell Signaling Technology, Danvers, MA, USA), APEX1 (A1117, ABclonal Technology, Woburn, MA, USA), XRCC1 (A0442, ABclonal), DCK (A1794, ABclonal), DCTD (16784-1-AP, Proteintech, Rosemont, IL, USA), FLAG (F1804, Sigma-Aldrich), FLAG (D6W5B, Cell Signaling Technology), PARP1 (46D11, Cell Signaling Technology), and PRIMPOL (https://pubmed.ncbi.nlm.nih.gov/36152632/).

Protein extractions and immunoblots

Cultured cells were collected by centrifugation, washed in 1 ml of ice-cold PBS, resuspended, and incubated in an equal volume of Benzonase buffer [20 mM tris-HCl (pH 8), 2 mM $MgCl_2$, 10% glycerol, 1% Triton X-100, and 12.5 U/ml of Benzonase] on ice for 10 min. Then, 2% sodium dodecyl sulfate was added (1:1, v/v) to the samples, followed by heating at 80°C for 2 min. Samples were resolved by polyacrylamide gel electrophoresis, transferred to nitrocellulose membranes, and incubated overnight with several antibodies.

RADAR assay

The RADAR assay was performed as previously described (*35*, *39*) with the following modifications. Cells were lysed in RADAR buffer [6 M guanidine thiocyanate, 1% sarkosyl, 4% Triton X-100, 1% 1,4-dithioerythritol, 10 mM tris (pH 6.5), and 20 mM EDTA (pH 8), adjusted to pH 6.5], and genomic DNA was isopropanol precipitated by the addition of 0.5× volume isopropanol and incubated for 15 min at −20°C. The DNA pellet was washed twice with 70% ethanol and resuspended in 8 mM NaOH. Samples were centrifuged to remove insoluble material, and then the DNA concentration was determined by spectrophotometry. Samples were then applied to nitrocellulose membrane with a slot blot apparatus. The membrane was blocked with 1% bovine serum albumin in TBST and immunoblotted for Flag epitope.

Cytotoxicity assays

Cells (2.5×10^3) were seeded in 96-well plates and incubated at 37°C overnight. The next day, the cells were exposed to increasing doses of 5hmdC for 72 hours. Viability was evaluated using Cell Proliferation Kit I (Roche, Basel, Switzerland) according to the manufacturer's instructions. Colorimetric analysis was performed using a Varioskan Flash plate reader (Thermo Fisher Scientific) at 550 nm.

Immunofluorescence microscopy

Cells (8×10^4) were seeded on coverslips (VWR, Radnor, PA, USA) in 24-well plates and incubated with the indicated drugs for the indicated times. Cells were preextracted in PBS + 0.25% Triton X-100 for 2 min on ice, fixed in PBS + 4% formaldehyde for 15 min on ice, blocked in PBS + 0.3% Tween 20 + 3% bovine serum albumin for 30 min, and incubated with primary antibodies overnight at 4°C.The next day, the cells were washed in PBS + 0.3% Tween 20 thrice and incubated with Alexa Fluor–labeled secondary antibodies of the chosen wavelength and DAPI (0.1 mg/ml) in PBS for 1 hour at room temperature (RT) in the dark. Last, the cells were washed three times with PBS + 0.3% Tween 20, and the coverslips were mounted in Prolong Gold Antifade Reagent (Thermo Fisher Scientific). For EdU immunofluorescence, cells were pulsed with EdU (10 μM) for 1 hour, and the click-it reaction (100 mM tris-HCl at pH 7.5, 1 μM Alexa Fluor 488 azide, 1 mM $CuSO_4$, and 100 mM ascorbic acid) was performed for 30 min at RT in the dark. At least 400 cells were analyzed per condition. Images were acquired at 40× on a THUNDER Imager DMi8 (Leica, Wetzlar, Germany) and then quantified and plotted using Fiji and GraphPad Prism 9.0 Software. Scale = 10 μm.

SIRF assay

SIRF assays were performed as previously described by Roy and Schlacher (*56*), with a few modifications. Briefly, 10^5 cells were seeded in coverslips, and the next day, EdU was added to the medium for 8 min. The cells were washed twice in PBS and then incubated in a medium containing 5hmdC (10 μM) for 3 hours. The cells were permeabilized in PBS + 0.5% Triton X-100 for 2 min at 4°C and fixed in PBS + 2% formaldehyde for 15 min at 4°C. Images of SIRF foci and cells were acquired at 63× on a THUNDER imager DMi8 (Leica) using LAS X, and the foci were quantified using Fiji. Scale = 10 μm.

Alkaline comet assay

Cells (2×10^5) were seeded in a six-well dish and treated as indicated. After treatment, the cells were collected, washed once in PBS, mixed with low–melting point agarose at a 1:5 ratio (v/v), and immediately layered onto prechilled frosted glass slides precoated with 0.6% agarose. The slides were allowed to settle in the dark at 4°C for at least 30 min, immersed in prechilled alkaline lysis buffer [10 mM tris-HCl (pH 10), 2.5 M NaCl, 100 mM EDTA, 1% (v/v) DMSO, and 1% (v/v) Triton X-100] for 1 hour at 4°C, and incubated in prechilled alkaline electrophoresis buffer [1 mM EDTA, 50 mM NaOH, and 1% (v/v) DMSO] for 30 min before electrophoresis at 0.6 V/cm for 25 min at 4°C. Following electrophoresis, the slides were neutralized with 0.4 M tris-HCl (pH 7) for 1 hour, stained with 1× SYBR Green I nucleic acid gel stain (Sigma-Aldrich, S9430) in PBS for 10 min, and visualized at 10× on a THUNDER imager DMi8 (Leica) using LAS X. Scale = 10 μm. Values represent the tail moments of comets determined using OpenComet.

Chromosome aberrations assays

Chromosome aberrations test was performed as previously described by Quinones and Demple (*15*).

SCE assays

Cells were grown in the presence of 10 μM BrdU during two cell cycles, and 5hmdC was added during the last 12 hours. Chromosomes were stained in 0.1 M phosphate buffer solution (pH 6.8) containing Hoechst (10 μg/ml) for 25 min. Slides were washed in McIlvaine's solution (164 mM Na_2HPO_4 and 15 mM citric acid) and exposed to ultraviolet light (365 nm) for 1 hour. After that, slides were incubated in 2× SSC solution (300 mM NaCl and 30 mM Na citrate) at 62°C for 1 hour and counterstained in phosphate buffer (pH 6.8) + 0.05% Tween20 + Leishman (1:4, v/v) for 3 min. To analyze SCEs, metaphase spreads were imaged at 100× using a DM6000 optical microscope (Leica) and analyzed using LAS AF (Leica) in a blinded manner.

DNA fiber assay

For replication fork blockage purposes, cells (7.5×10^4) were seeded and pulsed with CldU (20 μM) for 30 min and then with IdU (200 μM) in the presence of 5hmdC for a further 30 min. Cells (2 μl) were placed onto the slides, incubated for 6 min, and mixed with 7 μl of spreading buffer for further 30 min at RT. Slides were fixed in methanol/acetic acid (3:1) for 10 min, hydrated in PBS twice, and denatured in HCl (2.5 M) for 1 hour at RT. After washing and blocking, slides were incubated with primary and secondary antibodies. Last, slides were mounted in Fluoromount-G (eBioscience), scored with ×40 magnification lens Leica DM6000 fluorescence microscope using LAS AF Leica Software and analyzed using Fiji software. We plotted IdU/CldU ratio of each quantified fiber. To analyze asymmetry index, we measure length of both IdU tracks of each bidirectional fiber using Fiji software. Then, long versus short IdU track ratio of each bidirectional fiber is plotted using GraphPad Prism software.

DNA EM

DNA for EM analysis was processed as previously described (*20*, *47*). Briefly, for replication intermediates, cells (1.5×10^7) were collected and washed once with 5 ml of ice-cold PBS, resuspended in 10 ml of ice-cold PBS, and transferred to 10 × 5 mm petri dishes, to which trimethylpsoralen [10 mg/ml; thymidine 5′-monophosphate (TMP), Sigma-Aldrich] was added and mixed. Cell samples were incubated on ice for 5 min in the dark and irradiated with 365-nm ultraviolet light for 7 min on a precooled metal block. The procedure from TMP addition to irradiation with ultraviolet light was repeated four more times. Samples were then supplemented with 0.1% (w/v) SDS to lysate nuclei and treated with ribonuclease (100 μg/ml) for 1 hour at 37°C. For complete protein digestion, TMP–cross-linked chromatin was incubated with proteinase K (1 mg/ml) for 2 hours at 50°C. Genomic DNA was extracted by adding one volume of 1:1 (v/v) phenol-chloroform mixture, precipitated with isopropanol, washed with 70% ethanol and digested with 150 U of Pvu II HF restriction enzyme for 4 hours at 37°C. To visualize DNA, the samples were spread onto EM grids and stained as previously described (*20*, *47*). Briefly, 50 ng of DNA was resuspended in 5 μl of formamide supplemented with 0.4 μl of BAC solution [alkyl dimethyl benzyl ammonium chloride 0.2% (w/v) in formamide] diluted 1:10 (v/v) in water. The total volume was gently pipetted onto the surface of water in a petri dish to form a film. DNA was transferred to carbon-coated EM grids (Ted Pella) by briefly allowing them to contact the surface of the DNA film using tweezers. After staining in 1% uranyl acetate solution, followed by a brief wash in 100% ethanol, grids were air dried on filter paper and then subjected to DNA carbon-platinum rotary shadowing with a Leica MED20. Image acquisition was obtained with a FEI Tecnai 20 EM microscope equipped with a GATAN high-resolution camera at the IFOM EM facility. Blind analysis of EM images was performed by EM specialists. Conversion of DNA length from nanometers to nucleotides was done considering 1 nt = 0.34 nm under EM. Scale = 500 nt.

S1 nuclease fiber assay

S1 nuclease fiber assays were performed as previously described by Hanthi *et al.* (*47*), with a few modifications. Cells were incubated with CSK100 buffer [10 mM MOPS, pH 7, 100 mM NaCl, 3 mM $MgCl_2$ (pH 7.2), 300 mM sucrose, and 0.5% Triton X-100] for 5 min, washed with PBS, and treated with S1 nuclease (20 U/ml; Thermo Fisher Scientific, #EN0321) for 30 min at 37°C in S1 nuclease buffer [30 mM sodium acetate (pH 4.6), 10 mM zinc acetate, 5% glycerol, and 50 mM NaCl]. Then, the cells were washed with PBS and harvested with a scraper.

CRISPR-Cas9–mediated gene disruptions in RPE-1 cell lines

The single-guide RNAs targeting exon 2 of human *FANCD2* were previously reported (*15*). For *HMCES*, we used single-guide RNAs targeting exon 3 (HMCES-3.3, 5′-AUCAUUGCUCCCAUGCGCUG-3′; HMCES-3.8, 5′-UACGGUAUCACUACGACAGU-3′). Oligonucleotides containing the targeted sequences were cloned into pSpCas9-(BB)-2A-GFP (pX458, Addgene, plasmid no. 48138). After transfection, the cells were sorted, and single green fluorescent protein–positive (GFP^+) cells were seeded. Individual clones were analyzed for HMCES deletions using polymerase chain reaction. Gene disruption was confirmed by Sanger sequencing and Western blotting.

Analysis of prognosis

Kaplan-Meier survival plots stratified according to HMCES RNA sequencing expression data were obtained from the Kaplan-Meier Plotter database (https://kmplot.com/analysis/index.php?p= service) using the "Auto select best cutoff" option. Two different cohorts were analyzed: the breast adenocarcinoma cohort from The Cancer Genome Atlas (*57*) and a set of breast cancer curated cohorts (*53*). The significance of the differences between survival curves was estimated with the log-rank test.

Statistical analyses

In the total PAR and nuclear HMCES-FLAG plots, the center line represents the median value, whereas in EdU-PAR, foci per cell, and alkaline comet assay plots, it represents the means ± SD. Center line and boxes in DNA fiber assays represent median and 10th to 90th percentile, respectively. Statistical analyses were completed using Prism 8 (GraphPad). Analysis of variance (ANOVA) was used to compare more than two groups, followed by the Tukey or Fisher's least significant difference post hoc tests. No statistical methods or criteria were used to estimate sample size or to include/exclude samples. Unless otherwise stated, all experiments were performed in biological triplicates.

Supplementary Materials

This PDF file includes:

Figs. S1 to S12

REFERENCES AND NOTES

1. A. Tubbs, A. Nussenzweig, Endogenous DNA damage as a source of genomic instability in cancer. *Cell* **168**, 644–656 (2017).
2. T. Lindahl, An *N*-glycosidase from *Escherichia coli* that releases free uracil from DNA containing deaminated cytosine residues. *Proc. Natl. Acad. Sci. U.S.A.* **71**, 3649–3653 (1974).
3. E. Seeberg, L. Eide, M. Bjoras, The base excision repair pathway. *Trends Biochem. Sci.* **20**, 391–397 (1995).
4. T. Lindahl, DNA repair enzymes. *Annu. Rev. Biochem.* **51**, 61–87 (1982).
5. D. E. Barnes, T. Lindahl, B. Sedgwick, DNA repair. *Curr. Opin. Cell Biol.* **5**, 424–433 (1993).
6. T. Lindahl, Recognition and processing of damaged DNA. *J. Cell Sci. Suppl.* **19**, 73–77 (1995).
7. J. C. Fromme, G. L. Verdine, Base excision repair. *Adv. Protein Chem.* **69**, 1–41 (2004).
8. K. W. Caldecott, Mammalian DNA base excision repair: Dancing in the moonlight. *DNA Repair* **93**, 102921 (2020).
9. M. Garcia-Diaz, K. Bebenek, J. M. Krahn, L. Blanco, T. A. Kunkel, L. C. Pedersen, A structural solution for the DNA polymerase λ-dependent repair of DNA gaps with minimal homology. *Mol. Cell* **13**, 561–572 (2004).
10. P. J. McKinnon, K. W. Caldecott, DNA strand break repair and human genetic disease. *Annu. Rev. Genomics Hum. Genet.* **8**, 37–55 (2007).
11. K. W. Caldecott, Single-strand break repair and genetic disease. *Nat. Rev. Genet.* **9**, 619–631 (2008).
12. S. Mouron, S. Rodriguez-Acebes, M. I. Martinez-Jimenez, S. Garcia-Gomez, S. Chocron, L. Blanco, J. Mendez, Repriming of DNA synthesis at stalled replication forks by human PrimPol. *Nat. Struct. Mol. Biol.* **20**, 1383–1389 (2013).
13. A. Quinet, D. J. Martins, A. T. Vessoni, D. Biard, A. Sarasin, A. Stary, C. F. Menck, Translesion synthesis mechanisms depend on the nature of DNA damage in UV-irradiated human cells. *Nucleic Acids Res.* **44**, 5717–5731 (2016).
14. A. L. Piberger, A. Bowry, R. D. W. Kelly, A. K. Walker, D. Gonzalez-Acosta, L. J. Bailey, A. J. Doherty, J. Mendez, J. R. Morris, H. E. Bryant, E. Petermann, PrimPol-dependent single-stranded gap formation mediates homologous recombination at bulky DNA adducts. *Nat. Commun.* **11**, 5863 (2020).
15. J. L. Quinones, B. Demple, When DNA repair goes wrong: BER-generated DNA-protein crosslinks to oxidative lesions. *DNA Repair* **44**, 103–109 (2016).
16. S. H. Wilson, T. A. Kunkel, Passing the baton in base excision repair. *Nat. Struct. Biol.* **7**, 176–178 (2000).
17. A. Quinet, S. Tirman, E. Cybulla, A. Meroni, A. Vindigni, To skip or not to skip: Choosing repriming to tolerate DNA damage. *Mol. Cell* **81**, 649–658 (2021).
18. K. Cong, S. B. Cantor, Exploiting replication gaps for cancer therapy. *Mol. Cell* **82**, 2363–2369 (2022).
19. A. Taglialatela, G. Leuzzi, V. Sannino, R. Cuella-Martin, J. W. Huang, F. Wu-Baer, R. Baer, V. Costanzo, A. Ciccia, REV1-Polζ maintains the viability of homologous recombination-deficient cancer cells through mutagenic repair of PRIMPOL-dependent ssDNA gaps. *Mol. Cell* **81**, 4008–4025.e7 (2021).
20. A. Mann, M. A. Ramirez-Otero, A. De Antoni, Y. W. Hanthi, V. Sannino, G. Baldi, L. Falbo, A. Schrempf, S. Bernardo, J. Loizou, V. Costanzo, POLθ prevents MRE11-NBS1-CtIP-dependent fork breakage in the absence of BRCA2/RAD51 by filling lagging-strand gaps. *Mol. Cell* **82**, 4218–4231.e8 (2022).
21. O. Belan, M. Sebald, M. Adamowicz, R. Anand, A. Vancevska, J. Neves, V. Grinkevich, G. Hewitt, S. Segura-Bayona, R. Bellelli, H. M. R. Robinson, G. S. Higgins, G. C. M. Smith, S. C. West, D. S. Rueda, S. J. Boulton, POLQ seals post-replicative ssDNA gaps to maintain genome stability in BRCA-deficient cancer cells. *Mol. Cell* **82**, 4664–4680.e9 (2022).
22. H. E. Bryant, N. Schultz, H. D. Thomas, K. M. Parker, D. Flower, E. Lopez, S. Kyle, M. Meuth, N. J. Curtin, T. Helleday, Specific killing of BRCA2-deficient tumours with inhibitors of poly(ADP-ribose) polymerase. *Nature* **434**, 913–917 (2005).
23. H. Farmer, N. McCabe, C. J. Lord, A. N. Tutt, D. A. Johnson, T. B. Richardson, M. Santarosa, K. J. Dillon, I. Hickson, C. Knights, N. M. Martin, S. P. Jackson, G. C. Smith, A. Ashworth, Targeting the DNA repair defect in BRCA mutant cells as a therapeutic strategy. *Nature* **434**, 917–921 (2005).
24. P. X. Lim, M. Zaman, W. Feng, M. Jasin, BRCA2 promotes genomic integrity and therapy resistance primarily through its role in homology-directed repair. *Mol. Cell* **84**, 447–462.e10 (2024).
25. M. J. Pena-Gomez, P. Moreno-Gordillo, M. Narmonte, C. B. Garcia-Calderon, A. Ruksenaite, S. Klimasauskas, I. V. Rosado, FANCD2 maintains replication fork stability during misincorporation of the DNA demethylation products 5-hydroxymethyl-2′-deoxycytidine and 5-hydroxymethyl-2′-deoxyuridine. *Cell Death Dis.* **13**, 503 (2022).
26. M. J. Pena-Gomez, M. Suarez-Pizarro, I. V. Rosado, XRCC1 prevents replication fork instability during misincorporation of the DNA demethylation bases 5-hydroxymethyl-2′-deoxycytidine and 5-hydroxymethyl-2′-deoxyuridine. *Int. J. Mol. Sci.* **23**, 893 (2022).
27. K. Fugger, I. Bajrami, M. Silva Dos Santos, S. J. Young, S. Kunzelmann, G. Kelly, G. Hewitt, H. Patel, R. Goldstone, T. Carell, S. J. Boulton, J. MacRae, I. A. Taylor, S. C. West, Targeting the nucleotide salvage factor DNPH1 sensitizes *BRCA*-deficient cells to PARP inhibitors. *Science* **372**, 156–165 (2021).
28. A. Serrano-Benitez, S. E. Wells, L. Drummond-Clarke, L. C. Russo, J. C. Thomas, G. A. Leal, M. Farrow, J. M. Edgerton, S. Balasubramanian, M. Yang, C. Frezza, A. Gautam, J. Brazina, K. Burdova, N. C. Hoch, S. P. Jackson, K. W. Caldecott, Unrepaired base excision repair intermediates in template DNA strands trigger replication fork collapse and PARP inhibitor sensitivity. *EMBO J.* **42**, e113190 (2023).
29. S. Saxena, C. S. Nabel, T. W. Seay, P. S. Patel, A. S. Kawale, C. R. Crosby, H. Tigro, E. Oh, M. G. Vander Heiden, A. N. Hata, Z. Suo, L. Zou, Unprocessed genomic uracil as a source of DNA replication stress in cancer cells. *Mol. Cell* **84**, 2036–2052.e7 (2024).
30. S. Garcia-Gomez, A. Reyes, M. I. Martinez-Jimenez, E. S. Chocron, S. Mouron, G. Terrados, C. Powell, E. Salido, J. Mendez, I. J. Holt, L. Blanco, PrimPol, an archaic primase/polymerase operating in human cells. *Mol. Cell* **52**, 541–553 (2013).
31. E. Cybulla, A. Vindigni, Leveraging the replication stress response to optimize cancer therapy. *Nat. Rev. Cancer* **23**, 6–24 (2023).
32. K. Cong, M. Peng, A. N. Kousholt, W. T. C. Lee, S. Lee, S. Nayak, J. Krais, P. S. VanderVere-Carozza, K. S. Pawelczak, J. Calvo, N. J. Panzarino, J. J. Turchi, N. Johnson, J. Jonkers, E. Rothenberg, S. B. Cantor, Replication gaps are a key determinant of PARP inhibitor synthetic lethality with BRCA deficiency. *Mol. Cell* **81**, 3128–3144.e7 (2021).
33. A. Quinet, S. Tirman, J. Jackson, S. Svikovic, D. Lemacon, D. Carvajal-Maldonado, D. Gonzalez-Acosta, A. T. Vessoni, E. Cybulla, M. Wood, S. Tavis, L. F. Z. Batista, J. Mendez, J. E. Sale, A. Vindigni, PRIMPOL-mediated adaptive response suppresses replication fork reversal in BRCA-deficient cells. *Mol. Cell* **77**, 461–474.e9 (2020).
34. L. Halabelian, M. Ravichandran, Y. Li, H. Zeng, A. Rao, L. Aravind, C. H. Arrowsmith, Structural basis of HMCES interactions with abasic DNA and multivalent substrate recognition. *Nat. Struct. Mol. Biol.* **26**, 607–612 (2019).
35. K. N. Mohni, S. R. Wessel, R. Zhao, A. C. Wojciechowski, J. W. Luzwick, H. Layden, B. F. Eichman, P. S. Thompson, K. P. M. Mehta, D. Cortez, HMCES maintains genome integrity by shielding abasic sites in single-strand DNA. *Cell* **176**, 144–153.e13 (2019).
36. M. Srivastava, D. Su, H. Zhang, Z. Chen, M. Tang, L. Nie, J. Chen, HMCES safeguards replication from oxidative stress and ensures error-free repair. *EMBO Rep.* **21**, e49123 (2020).
37. M. Donsbach, S. Durauer, F. Grunert, K. T. Nguyen, R. Nigam, D. Yaneva, P. Weickert, R. Bezalel-Buch, D. R. Semlow, J. Stingele, A non-proteolytic release mechanism for HMCES-DNA-protein crosslinks. *EMBO J.* **42**, e113360 (2023).
38. J. Rua-Fernandez, C. A. Lovejoy, K. P. M. Mehta, K. A. Paulin, Y. T. Toudji, C. Giansanti, B. F. Eichman, D. Cortez, Self-reversal facilitates the resolution of HMCES DNA-protein crosslinks in cells. *Cell Rep.* **42**, 113427 (2023).
39. D. Yaneva, J. L. Sparks, M. Donsbach, S. Zhao, P. Weickert, R. Bezalel-Buch, J. Stingele, J. C. Walter, The FANCJ helicase unfolds DNA-protein crosslinks to promote their repair. *Mol. Cell* **83**, 43–56.e10 (2023).
40. K. P. M. Mehta, C. A. Lovejoy, R. Zhao, D. R. Heintzman, D. Cortez, HMCES maintains replication fork progression and prevents double-strand breaks in response to APOBEC deamination and abasic site formation. *Cell Rep.* **31**, 107705 (2020).
41. A. Taglialatela, S. Alvarez, G. Leuzzi, V. Sannino, L. Ranjha, J. W. Huang, C. Madubata, R. Anand, B. Levy, R. Rabadan, P. Cejka, V. Costanzo, A. Ciccia, Restoration of replication fork stability in BRCA1- and BRCA2-deficient cells by inactivation of SNF2-family fork remodelers. *Mol. Cell* **68**, 414–430.e8 (2017).
42. A. Masaoka, M. Matsubara, R. Hasegawa, T. Tanaka, S. Kurisu, H. Terato, Y. Ohyama, N. Karino, A. Matsuda, H. Ide, Mammalian 5-formyluracil-DNA glycosylase. 2. Role of SMUG1 uracil-DNA glycosylase in repair of 5-formyluracil and other oxidized and deaminated base lesions. *Biochemistry* **42**, 5003–5012 (2003).
43. T. C. Liu, C. T. Lin, K. C. Chang, K. W. Guo, S. Wang, J. W. Chu, Y. Y. Hsiao, APE1 distinguishes DNA substrates in exonucleolytic cleavage by induced space-filling. *Nat. Commun.* **12**, 601 (2021).
44. P. Burkovics, I. Hajdu, V. Szukacsov, I. Unk, L. Haracska, Role of PCNA-dependent stimulation of 3′-phosphodiesterase and 3′-5′ exonuclease activities of human Ape2 in repair of oxidative DNA damage. *Nucleic Acids Res.* **37**, 4247–4255 (2009).
45. A. A. Demin, K. Hirota, M. Tsuda, M. Adamowicz, R. Hailstone, J. Brazina, W. Gittens, I. Kalasova, Z. Shao, S. Zha, H. Sasanuma, H. Hanzlikova, S. Takeda, K. W. Caldecott, XRCC1 prevents toxic PARP1 trapping during DNA base excision repair. *Mol. Cell* **81**, 3018–3030.e5 (2021).
46. J. Biayna, I. Garcia-Cao, M. M. Alvarez, M. Salvadores, J. Espinosa-Carrasco, M. McCullough, F. Supek, T. H. Stracker, Loss of the abasic site sensor HMCES is synthetic lethal with the activity of the APOBEC3A cytosine deaminase in cancer cells. *PLOS Biol.* **19**, e3001176 (2021).
47. Y. W. Hanthi, M. A. Ramirez-Otero, R. Appleby, A. De Antoni, L. Joudeh, V. Sannino, S. Waked, A. Ardizzoia, V. Barra, D. Fachinetti, L. Pellegrini, V. Costanzo, RAD51 protects abasic sites to prevent replication fork breakage. *Mol. Cell* **84**, 3026–3043.e11 (2024).
48. Y. Lin, J. Raj, J. Li, A. Ha, M. A. Hossain, C. Richardson, P. Mukherjee, S. Yan, APE1 senses DNA single-strand breaks for repair and signaling. *Nucleic Acids Res.* **48**, 1925–1940 (2020).
49. M. A. Hossain, Y. Lin, G. Driscoll, J. Li, A. McMahon, J. Matos, H. Zhao, D. Tsuchimoto, Y. Nakabeppu, J. Zhao, S. Yan, APE2 is a general regulator of the ATR-Chk1 DNA damage

response pathway to maintain genome integrity in pancreatic cancer cells. *Front. Cell Dev. Biol.* **9**, 738502 (2021).
50. A. Brambati, O. Sacco, S. Porcella, J. Heyza, M. Kareh, J. C. Schmidt, A. Sfeir, RHINO directs MMEJ to repair DNA breaks in mitosis. *Science* **381**, 653–660 (2023).
51. Y. Sugimoto, Y. Masuda, S. Iwai, Y. Miyake, R. Kanao, C. Masutani, Novel mechanisms for the removal of strong replication-blocking HMCES- and thiazolidine-DNA adducts in humans. *Nucleic Acids Res.* **51**, 4959–4981 (2023).
52. R. Zellweger, D. Dalcher, K. Mutreja, M. Berti, J. A. Schmid, R. Herrador, A. Vindigni, M. Lopes, Rad51-mediated replication fork reversal is a global response to genotoxic treatments in human cells. *J. Cell Biol.* **208**, 563–579 (2015).
53. B. Gyorffy, Survival analysis across the entire transcriptome identifies biomarkers with the highest prognostic power in breast cancer. *Comput. Struct. Biotechnol. J.* **19**, 4101–4109 (2021).
54. A. Hale, A. Dhoonmoon, J. Straka, C. M. Nicolae, G. L. Moldovan, Multi-step processing of replication stress-derived nascent strand DNA gaps by MRE11 and EXO1 nucleases. *Nat. Commun.* **14**, 6265 (2023).
55. N. Garcia-Rodriguez, I. Dominguez-Garcia, M. D. C. Dominguez-Perez, P. Huertas, EXO1 and DNA2-mediated ssDNA gap expansion is essential for ATR activation and to maintain viability in BRCA1-deficient cells. *Nucleic Acids Res.* **52**, 6376–6391 (2024).
56. S. Roy, K. Schlacher, SIRF: A single-cell assay for in situ protein interaction with nascent DNA replication forks. *Bio Protoc.* **9**, e3377 (2019).
57. G. Ciriello, M. L. Gatza, A. H. Beck, M. D. Wilkerson, S. K. Rhie, A. Pastore, H. Zhang, M. McLellan, C. Yau, C. Kandoth, R. Bowlby, H. Shen, S. Hayat, R. Fieldhouse, S. C. Lester, G. M. Tse, R. E. Factor, L. C. Collins, K. H. Allison, Y. Y. Chen, K. Jensen, N. B. Johnson, S. Oesterreich, G. B. Mills, A. D. Cherniack, G. Robertson, C. Benz, C. Sander, P. W. Laird, K. A. Hoadley, T. A. King, T. R. Network, C. M. Perou, Comprehensive molecular portraits of invasive lobular breast cancer. *Cell* **163**, 506–519 (2015).

Acknowledgments: RPE-1 *TP53*$^{-/-}$ or DLD-1 BRCA2$^{-/-}$ cell lines were provided by P. Huertas (University of Seville/CABIMER, Spain) and A. Aguilera (University of Seville/CABIMER, Spain), respectively. We thank F. Zhang (Broad Institute, USA) and H. Leonhardt (LMU, Munich) for providing the pSpCas9(BB)-2A-GFP (Addgene, #48138) and pCAG-BSR plasmids, respectively. We also acknowledge N. St-Denis (High-Fidelity Science Communications Ltd.) for manuscript edition. We are in debt to J. Duxin (Novo Nordisk Foundation Center for Protein Research, U. Copenhagen, DK), G. P. Crossan (Astra Zeneca, UK), and L. B. Pontel (Instituto Josep Carreras, Spain) for critical reading of the manuscript and M. Giannattasio of the IFOM DNA EM facility for assistance. **Funding:** This publication is part of the project PID2021-128988OB-I00, funded by MICIU/AEI/10.13039/501100011033 and by ERDF/EU. This research work was also supported by CNS2022-136055 financiado por MCIN/AEI/10.13039/501100011033/UniónEuropeaNextGenerationEU/PRTR. J.Y.M. is a Tier I Canada Research Chair in DNA Repair and Cancer Therapeutics and was supported by a Canadian Institutes of Health Research Foundation Grant (FDN-388879). V.C. received funding from AIRC under IG 2023-ID 28725 project. M.J.P.-G. was supported by Consejería de Transformación Económica, Industria, Conocimiento y Universidades (PREDOC_00505). Y.R.-M. was supported by PID2021-128988OB-I00/MCIN/AEI/10.13039/501100011033/FEDER, UE. M.d.R.O. was supported by CNS2022-136055/MCIN/AEI/10.13039/501100011033/Unión Europea NextGenerationEU/PRTR. Y.W.H. was supported by the 26596 AIRC fellowship for Italy. S.B. is supported by an FRQ-S postdoctoral fellowship. **Author contributions:** M.J.P.-G.: Investigation and methodology, data curation, validation, formal analysis, and visualization. Y.R.-M.: Investigation, validation, formal analysis, and visualization. M.d.R.O.: Investigation, methodology, validation, formal analysis, and visualization. Y.W.H.: Investigation, methodology, data curation, validation, formal analysis, and visualization. S.B.: Investigation and writing—review and editing. R.F.: Writing—review and editing and resources. J.Y.M.: Writing—review and editing, funding acquisition, and supervision. J.C.R.: Investigation. V.C.: Conceptualization, investigation, writing—review and editing, resources, funding acquisition, and supervision. I.V.R.: Writing—original draft, conceptualization, investigation, writing—review and editing, methodology, resources, funding acquisition, data curation, validation, supervision, formal analysis, project administration, and visualization. **Competing interests:** The authors declare that they have no competing interests. **Data and materials availability:** All data needed to evaluate the conclusions in the paper are present in the paper and/or the Supplementary Materials. Raw data are available at Zenodo (https://zenodo.org/records/14738090).

Submitted 7 August 2024
Accepted 21 February 2025
Published 26 March 2025
10.1126/sciadv.ads3227